Characterisation of reaction propagation from auto-ignition.

By Luke Robert Bates

MEng

Submitted in accordance with the requirements for the degree of *Doctor of Philosophy.*

The University of Leeds
School of Mechanical Engineering
July 2016

The candidate confirms that the work submitted is his own, except where work which has formed part of jointly authored publications has been included. The contribution of the candidate and the other authors to this work has been explicitly indicated below. The candidate confirms that appropriate credit has been given within the thesis where reference has been made to the work of others.

Figures 4-2, 4-5, 4-6, in Chapter 4 and 5-3 in Chapter 5 have appeared in the jointly authored paper:

L. Bates, D. Bradley, G. Paczko, N. Peters, “Engine Hot Spots: Modes of Auto-ignition and Reaction Propagation," Combust. Flame 166 (2016) 80-85.

And also in:

L. Bates, D. Bradley, G. Paczko, N. Peters. *Engine Hot Spots: Decay, Deflagration, Auto-Ignitive Propagation, or Detonation?* International Colloquium on Combustion, Detonation and Reacting Systems, Leeds, United Kingdom, 2015
I was responsible for all figures and jointly responsible for writing the text with Prof D. Bradley. The remaining authors provided data, which is referenced, and editorial comments.

Figures 5-1 and 5-2, in Chapter 5 and 6-2, 6-3, and 6-4 in Chapter 6 have appeared in the jointly authored paper:

Bates, L., Bradley, D. *Deflagrative, auto-ignitive, and detonative propagation regimes in engines* (2017) Combustion and Flame, 175, pp. 118-122.

I was responsible for all figures and jointly responsible for writing the text with Prof D. Bradley.

Acknowledgements

The completion of this work would not have been possible without the support of others, too many to mention here. My thanks go out to all who have helped, wittingly or not.

Thanks are expressed to my family for their support and encouragement in completing this thesis (Including many “blah blahs” when attempting to proof read). To Dr Richard Mumby, who provided many interesting conversations, combustion related and otherwise, and who let me get my hands dirty in the lab when a computer screen became too repetitive, a very welcome therapy. To Dr Myeji Matarego for his constant cheerfulness and auto-ignition discussions. Dr Scott Dunkley for baffling me with maths then suddenly making the principles make sense. To Ben Thorne who despite excessive humility has provided many interesting avenues of discussion through his work, and for the honey. In addition, to Inna Gorbatenko who reinvigorated a direction of my work that had, to some extent, stagnated. I thank you all.

My warm thanks go to Professor Derek Bradley, whose guidance and unrelenting and infectious enthusiasm for research were essential to the completion of this work. I hope to have helped in an ambition to “kill off” the octane number.

My thanks are also due to Dr Malcolm Lawes for his ever practical advice and supervision; and to Dr Gary Sharpe, who began this journey but was unable to see it to its end; I wish you good fortune in your future pursuits.

Abstract

Finite supplies of fossil fuels and their current dominance in energy production and usage make their efficient usage and the search for viable alternatives of critical importance. A large part of this is the understanding of the combustion of fuels, both existing and novel and of the engines in which they are consumed.

One fundamental parameter that is not sufficiently understood is excitation time, the almost instantaneous heat release period at the end of an ignition delay period. A reduced thermokinetic model is applied to an attempt to simulate excitation without a large comprehensive model. The failure of the model in this task indicates differences in chemistry between excitation and ignition delay periods that are too large for a simple scheme to overcome with a single set of rate parameters.

This work will present a full and fundamental characterisation through the use of two complimentary diagrams, one an existing diagram for the identification of developing detonation, the other for turbulent burning and adapted to this purpose for the first time. The ε/ξ diagram has been developed with additional groups and parameters which aid in identifying regimes which are potentially beneficial and also those that might be damaging. The newly developed U/K diagram additionally allows the application of the ε/ξ diagram in turbulent burning conditions.

The diagrams are able to identify various combustion modes, including bounds between deflagrative and auto-ignitive propagation and operating regimes for specific engines.

Contents

List of Figures

List of Tables

Nomenclature

a	acoustic speed (m s^{-1})	U	turbulent burning velocity normalised by rms turbulent velocity.
c	dimensionless constant with given values of u_l, a, l and ν.	u_a	Auto-ignition velocity (m s^{-1})
E	activation energy (J mol^{-1})	u_l	laminar burning velocity (m s^{-1})
$\bar{E}$	detonation stability dimensionless group, ($\bar{E}=(\tau_i/\tau_e)(E/RT)$)	u_t	turbulent burning velocity (m s^{-1})
K	Karlovitz turbulent flame stretch factor	u'	rms turbulent velocity (ms^{-1})
l	turbulent length scale (m)	***Greek***	
Ma_{sr}	strain rate Markstein number	ε	Residence time of pressure wave in hot spot normalised by excitation time ($\varepsilon = r_o/a\tau_e$).
P	Pressure (Pa)	ν	Kinematic viscosity ($m^2\ s^{-1}$)
R	ideal gas constant (J mol^{-1} K^{-1})	ξ	Acoustic speed normalised by auto-ignition velocity ($\xi = a/u_a$).
R	distance along r_o (m)	τ_e	Excitation time (s)
r_o	hot spot radius (m)	τ_i	Ignition delay time (s)
$\bar{r}$	normalised hotspot radius	ϕ	Equivalence ratio
T	temperature (K)		

1 Introduction

1.1 *Overview and Motivation*

Currently known reserves of fossil fuels are dominated by coal, which Dry (2002) lists as 15 times more abundant than crude oil. Natural gas is only 1.5 times more abundant than crude oil. As these reserves are depleted, it becomes increasingly important to both find alternative energy sources and to use the remaining supply as efficiently as possible.

Bradley et al. (2009) states that transport makes up 36% of energy consumption in the UK, almost all of which is derived from fossil fuels, especially crude oil. While alternative options for propulsion are available, limitations with existing technologies and electricity generation largely based upon fossil fuels limits the viability of these alternatives in many applications. The combustion of liquid fuels remains practical because of the relatively high volumetric and gravimetric energy densities of many liquid fuels.

One option for the reduction of crude oil dependence of transport is to use an alternative fuel. Examples of possible alternatives include bio-fuels produced from plant matter or algae, or utilization of more abundant coal through gasification and the Fischer–Tropsch process.

Making the best use of the existing reserves and utilizing new alternatives while maintaining safety during transport and storage requires considerable understanding of the fuels.

Efficiency in engines has also been the subject of considerable effort, including both the improvement of existing engine designs and the development of new engine types. These include the downsizing and turbocharging of internal combustion, IC, engines, and the development of engines such as the controlled Auto-Ignition Engine, CAI, also described as the Homogeneous Charge Compression Ignition engine, HCCI. These will be referred to here as CAI engines due to the practical impossibility of a homogeneous charge.

Downsized engines are smaller in capacity but with increased specific power output through boosting. The smaller capacity of the engine allows it to be run closer to maximum load when compared to a larger naturally aspirated gasoline engine during the majority of automotive use (Li et al. 2014). This reduces the losses incurred by throttling the air intake into the engine at low loads. Workers at Jaguar Land Rover (Turner et al., 2014) recorded a 23% improvement in fuel consumption with a Downsizing Factor, *DF* of 60%, where the downsizing factor is defined as:

$$DF = (V_{swept_{NA}} - V_{swept_{DS}})/V_{swept_{NA}} \quad (1)$$

Where $V_{swept_{NA}}$ is the swept volume of a naturally aspirated engine of a given power output, and $V_{swept_{DS}}$ is the swept volume of a downsized engine with similar power output (Turner et al. 2014). As specific output is increased through boosting, the propensity for knock is also increased. This can be alleviated through reduction of the compression ratio, but at the cost of part-load efficiency (Fraser, 2009). Direct injection is an alternative solution to this issue, as the latent heat of evaporation of the fuel cools the charge, which both reduces the risk of knock and increases the density of the charge, improving volumetric efficiency.

CAI engines operate without the use of spark ignition by auto-ignition of the fuel charge. This can occur at multiple sites within the cylinder, rather than the single ignition point of a conventional spark-ignited gasoline engine. Combustion in CAI engines operates under stoichiometric or fuel lean conditions, with Exhaust Gas Recirculation, EGR, often implemented as a means to dilute and simultaneously heat the fuel-air mixture (Cairns & Blaxill, 2005). The ability of such engines to operate at wide-open throttle under part load contributes to an improved thermal efficiency of up to ~45%, compared to a conventional SI engine thermal efficiency of ~25% (Cairns & Blaxill, 2005). CAI engines also offer low NOx and particulate emissions (Brands, 2014) but controlling their operation across a wide range of operating conditions is problematic.

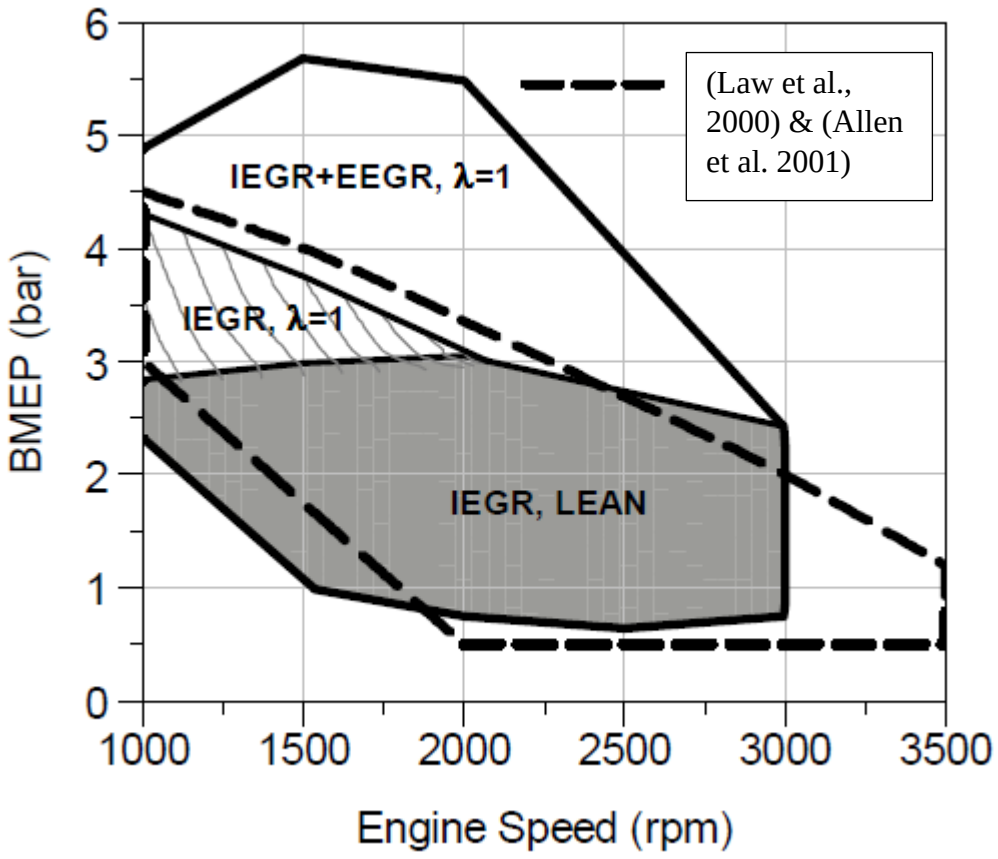

Figure 1.1: BSFC diagram comparing two CAI engine studies (Cairns & Blaxill, 2005)

ε1 shows a Brake Specific Fuel Consumption, BSFC, diagram (Cairns & Blaxill, 2005) that compares the results of two CAI studies. The dashed outlined region shows the operating range of a single cylinder research engine with fully variable valve timing operating as a stoichiometric CAI engine (Law et al., 2000) , (Allen et al., 2001). The grey shaded region, which extends to slightly lower speeds for given load is the operating range achieved by Cairns & Blaxill (2005) with lean a burning CAI engine with exhaust gas recirculation. This is extended to higher loads in the crosshatched region by moving stoichiometric combustion and further into the white outlined region with the addition of external exhaust gas recirculation. Neither study was able to operate at low speed and load, below ~1500 rpm and Brake Mean Effective Pressure, BMEP, below ~1.5 bar.

Much like new fuels, the development and best application of an engine requires considerable understanding of its behaviour under varying conditions, making the full and comprehensive characterization of both fuels and engines important. This thesis will present a characterisation methodology, which can address both the characterisation of both fuels and engines.

1.2 Increasing engine efficiency

A limiting factor to efficiency in internal combustion engines is knock. Knock is a term sometimes used synonymously with detonation, but is a distinct phenomenon. It is defined by Miller (1947) as “objectionable noise outside the engine” and is caused by auto-ignition in the unburned and compressed gas in the engine cylinder ahead of the propagating flame front. This creates a pressure pulse which may be benign, having

insufficiently strong pressure pulse or heat flux to cause damage, or in extreme cases may cause terminal damage (Nates & Yates, 1994). Such an extreme case is shown in Fig. 1.2, (Bradley & Morely, 1997) where high intensity pressure pulses and heat flux have severely damaged an engine piston.

Figure 1.2 Knock damage sustained by an engine piston, from Bradley and Morley (1997)

The auto-ignition that causes knock can be thought of as a relatively simple fuel property. For a given fuel air mixture, the auto-ignition delay time, τ_i, is a function of temperature, T, and pressure, P.

$$\tau_i = f(P,T) \quad (2)$$

The auto-ignition delay time is the period during which a given fuel air mixture at a given T and P reacts with negligible heat release before ignition occurs as a near instantaneous heat release. In general, higher T and P results in a smaller τ_i, making ignition, and so knock, at a point in the unburned gas more probable in the period before that point is engulfed by the flame front.

To increase the efficiency of the engine the compression ratio, and hence expansion ratio, needs to increase (Akihisa and Daisaku 2010). However, this also increases temperature and pressure, making auto-ignition and therefore potentially damaging knock more likely. In addition, engine compression ratio is limited by mechanical and geometric considerations due to rotating weight and the required piston speed. This results in a practical compression ratio limit of around 14. This limitation to compression ratio can be overcome to some extent by the Miller cycle, where the expansion ratio is increased relative to the compression ratio. The compression ratio can be reduced by varying the intake valve timing, reducing the end of compression T and P, and so limiting knock (Li et al. 2014). The Miller cycle can lead to efficiency gains at lower loads due to reduced frictional losses.

Fuels have varying degrees of resistance to knock, a more resistant fuel allowing a higher compression ratio and more efficient engine makes it important to have a method for characterisation of the anti-knock qualities of fuels. In the late 1920s, a rating system for gasoline engine fuels was proposed based on the anti-knock performance of mixtures of primary reference fuels, PRF. The chosen constituents were *i*-octane and *n*-heptane, both paraffins with contrasting performance in gasoline engines. The fuel would be given an octane number based on the percentage by liquid volume of i-octane in the PRF blend that exhibited the same anti-knock performance

as the tested fuel (Bradley & Head, 2006). This reference fuel test still has the limitation of rating the combination of both engine and fuel. To rectify this specifically tasked single cylinder, variable compression ratio engines were developed with the aim of isolating the fuel performance.

The Ron test mandates an engine speed of 600 rpm, intake mixture temperature of 52 °C and spark timing of 13° before TDC (ASTM D2699-16, 2016). The MON test, with much more severe conditions, including an engine speed of 900 rpm and intake mixture temperature of 149 °C (ASTM D2700-16a, 2016) was later developed when the RON system was found to offer poor correlation with engines at the time (Bradley & Morley, 1997).

This system for rating fuels has been widely adopted and is still very much in use around the world. However, the system, while prevalent, has several serious flaws, not least the development of both engines and fuels over the last eight decades. Modern engines have higher compression ratios for a given aspiration type, run at different temperatures and pressures with much more knock resistant fuels than those contemporary with the RON and MON tests. There is also a problem in that any fuel more knock able than *n*-heptane, or more resistant than *i*–octane requires extrapolation to an octane number of a PRF mixture that cannot exist. The ratings have been adapted in several ways to accommodate these flaws, for example in the United States of America the mean value of the two ratings, (RON+MON)/2 is used and termed the anti-knock index, AKI. Kalghatgi (2001, 2015) also suggests an empirical correction factor, *K*, which is expressed as:

$$OI = RON - K\,(RON - MON). \quad (3)$$

Where OI is the Octane Index, the empirically corrected value for Octane Number, ON. The *K* in Equation (3) should not be confused with that in Chapter 6, which is the Karlovitz stretch factor. Kalghatgi (2001) observed a general trend of a negative *K* factor in a study of contemporary cars. This suggests that fuels with a high sensitivity offer increased knock limited performance despite often having lower MON values. High sensitivity fuels, such as ethanol, which has both a high sensitivity of ~17.8, and a high RON of ~109 (Foong et al., 2014), have been highlighted as important to the development of future engines due to the potential improvements offered by a high OI (Morgan et al., 2010).

A method similar to that of Octane Number, ON, rating has been the employment of further surrogate fuels in an attempt to replace octane numbers. Commonly these surrogates include toluene, an aromatic, to reflect the presence of aromatics in gasoline and to increase the maximum knock resistance of the surrogate fuel. These approaches attempt to create fuels that are more like real gasolines, and so give results that are more useful at engine conditions than current PRFs.

Another alternative approach considers the more fundamental properties of the fuel, such as ignition delay and excitation time, τ_i and τ_e respectively. This approach focuses on the origin of the potentially damaging knock, which is a hotspot. These hotspots arise for a number of reasons; such as fuel mixture inhomogeneity, or local temperature gradients caused by hot recirculated gases or hot walls close to an exhaust valve. These hot spot temperature gradients can give rise to an auto-ignition velocity, u_a as the ignition delay varies constantly along the temperature gradient, as shown by Zel'dovich (1980). If the auto-ignition velocity is sufficiently close to the sound speed in the mixture, the pressure pulse created by the auto-ignition can be reinforced by reaction heat release and accelerated to detonation. The dimensionless group ξ is

therefore expressed as $\xi = a/u_a$, where a is sound speed and u_a auto-ignition velocity. If ξ has a value close to unity, the rate of propagation of both pressure pulse and reaction front is similar, and a detonation resulting from reinforcement of the pressure pulse by heat release is likely.

1.3 Measuring auto-ignition delay

There are two main apparatus used for the measurement of auto-ignition delay time, rapid compression machines, RCM, and shock tubes. A shock tube is a simple apparatus that can be used to experimentally study auto-ignition in fuels. The principle of shock tubes is to use a high pressure differential to degenerate a shock wave. This shock wave travels into the low pressure gas supersonically (Turns, 2006).

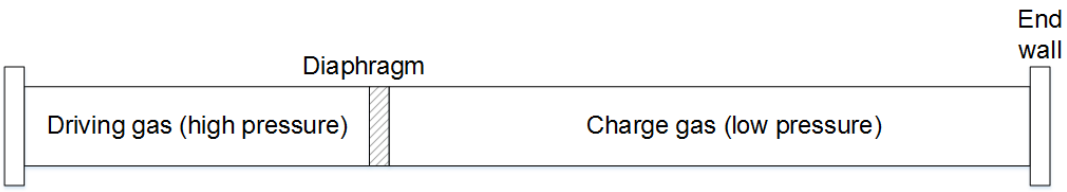

Figure 1.3: Simplified diagram of a shock tube.

Shock tubes, as in Fig. 1.3 consist of a tube with a diaphragm separating one end from the other. In one section of the tube the pressure and temperature is raised. The other section of tube is kept at low pressure and temperature and contains a low concentration of fuel charge. The auto-ignition will be initiated by a shock wave, produced by piercing the diaphragm that separates the driving gas from the test gas (Griffiths, 1996). The instantaneous pressure differential causes a shock wave to develop and move into the test gas. As this shock wave propagates supersonically

through the test gas, the gas is instantaneously heated to high temperature. The shock wave is followed by a contact surface between the test gas and driver gas. This sub-sonic contact surface moves into the area that was previously occupied by the test gas. A rarefaction, or expansion stage, follows this, cooling the gasses.

The diaphragm can be burst or pierced in a number of ways. Most simply a mechanical plunger can be used to pierce the diaphragm, alternatively an explosive charge can also be used to burst through the diaphragm or the diaphragm can be designed to rupture at a pre-determined pressure differential. It is desirable for the removal of the diaphragm to occur as quickly as possible (White, 1958).

Due to the design of shock tubes, some issues exist with their use (Chaos & Dryer, 2010). Simple shock tubes have closed ends. These closed ends reflect the shockwave back into the test gas before the rarefaction wave arrives, which results in the effected gas being doubly heated. The propagation of the shock wave is also not ideal. The shock wave is effected by factors such as the viscosity of the gas charge and the boundary layers close to the tube walls. Experimental data requires adjustment to account for these effects (Chaos & Dryer, 2010). The time over which the reaction can be reliably observed is limited, and varies between machines. This time period may be as little as 10 - 1000μs (Griffiths 1996). The shorter end of this scale allows little time for reaction to take place, some shock tubes will be unable to reach ignition in fuels with longer delay times.

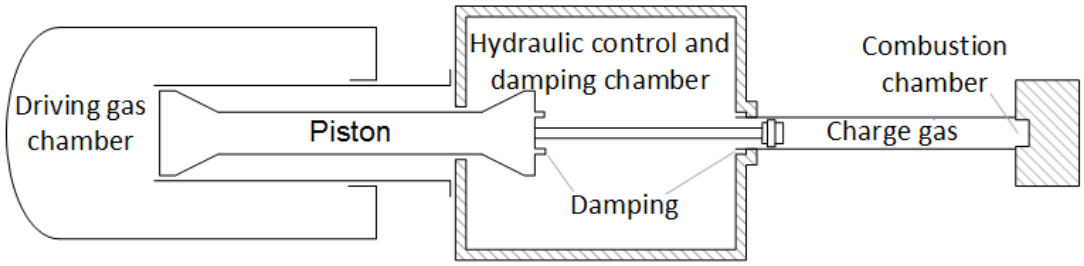

Figure 1.4: Simplified diagram of an RCM

Rapid Compression Machines, RCMs, such as that shown in Fig 1.4, are, in principle, simple devices. An initial volume containing the fuel and air charge is compressed at high speed by a piston or pistons (Bhari, 2010). At the end of the compression, Top Dead Centre (TDC) is reached and the piston is stopped. The gas in the RCM chamber is now termed the end gas. The compression is sufficient to raise the temperature and pressure such that auto-ignition in the end gas occurs (Lee, 1998). This process can be thought of in terms of a single compression event in an internal combustion piston engine. Because the piston is held at TDC, the potential reaction time is much longer than that of shock tubes.

The Leeds RCM, shown in Fig. 1.5, uses a single piston, which is driven by pressurised gas and damped hydraulically. Alternative designs such as dual opposing piston configurations, with twin opposing designs such as that of Wurmel and Simmie (2005) also exist.

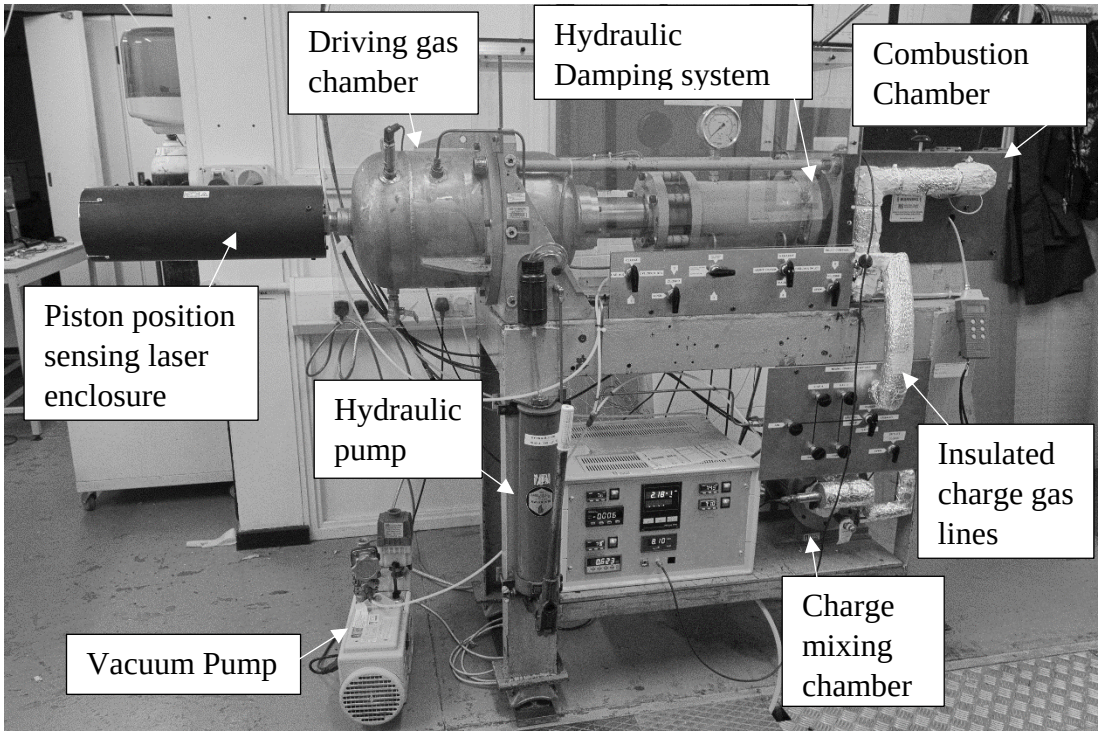

Figure 1.5: The Leeds Rapid Compression Machine.

One of the most critical features of an RCM's design is the damping at the end of compression. This is because, while it is relatively simple to propel the piston at high speed along the cylinder, it is very difficult to bring it to a controlled but rapid stop at TDC. This can result in the piston bouncing back from TDC, and so effecting the pressure and temperature of the reaction chamber. Damping can be achieved by some conventional methods such as hydraulic damping as in the Leeds RCM, but other methods have also been attempted, such as the compression and deformation of sacrificial dampers like those of Watanabe (2008).

1.4 Comprehensive modelling of auto-ignition

Comprehensive mechanisms for auto-ignition delay modelling attempt to accurately reproduce every chemical reaction involved in the process of combustion. Even for a

relatively simple pure fuel the number of these reactions can reach the hundreds. Out of necessity, modelling of comprehensive schemes started with small molecule fuels in order to minimise the number of reactions involved (Westbrook & Dryer, 1981). These relatively simple schemes can then be used as a foundation for mechanisms involving larger molecules, such as those of Westbrook & Dryer (1984) and Warnatz (1984), for which the reaction set of the smaller molecules is encapsulated within that of the larger molecules. This makes the comprehensive modelling of large fuel molecules a lengthy, staged process which to date has taken several decades. Increasingly optimised software, such as Chemkin, coupled with ever more powerful and available computers has prompted a shift to more automated computationally generated schemes (Bradley 1997).

While detailed models are comprehensive in their reaction set, they are by no means certain. For every reaction rate constant, there is a small level of uncertainty; empirical corrections are often applied within even comprehensive schemes for fuels that are considered to have well understood kinetics (Cai et al. 2016). Individually these uncertainties are negligible, but cumulatively in a very large scheme, they could lead to significant errors.

1.5 Reduced modelling of auto-ignition

Contrary to the very complex comprehensive mechanisms, much simpler methods have been used to replicate auto-ignition delay times. The Livengood-Wu integral (Livengood & Wu, 1955) is the result of the assumption that the intermediate compounds' concentration is the sum of the compounds produced at every condition of pressure and temperature in the lead up to ignition:

$$\int_{t_1}^{t_2} dt/\tau_{i_{(P,T)}} = N_i \quad (3)$$

Where τ_i, as in Eqn. 1, is the ignition delay time as a function of *T*, temperature and *P*, pressure. As the integration progresses the reciprocal of ignition delay at each time step is added. This reciprocal is the proportion of required brewing reaction required for ignition that has occurred during the time step. Auto-ignition occurs at the point where the dimensionless result of the integral, N_i, is equal to unity, or when the entire brewing reaction process has completed. The Arrhenius equation can also be used to represent auto-ignition delay as a single reaction rate and takes the form:

$$\tau_{i_{(P,T)}} = Aexp - (E_a/RT) \quad (4)$$

Where *A* is a constant referred to as the pre-exponential factor, *R* is the Universal Gas Constant, *T* is temperature, and *Ea* is activation energy. The Livengood-Wu integral and Arrhenius equation use a single global equation for the reaction rates, which limits their ability to reproduce real fuels, they cannot account, for example, for slower cool flame reactions or the NTC region exhibited by some fuels.

The problems associated with the large equation sets of comprehensive mechanisms have prompted the development of so-called reduced or generalized mechanisms. These much smaller mechanisms have many less reactions than an equivalent comprehensive scheme. They attempt to represent entire groups of species and reactions to reproduce the macroscopic behaviour of the fuel, rather than the minute detail of the chemistry.

Reaction	Reaction Type	Reaction Process
1	Initiation	$RH + O_2 \rightarrow 2R + Products$
2	Propagation	$R \rightarrow R + heat$
3	Formation of Branching Agent	$R \rightarrow R + B$
4	Formation of Reactive Intermediate	$R \rightarrow R + Q$
5	Linear Termination	$R \rightarrow Products$
6	Quadratic Termination	$2R \rightarrow Products$
7	Branching	$B \rightarrow 2R$
8	High Temperature Chain	$R + Q \rightarrow R + B$

Table 1.1: The Shell model reaction scheme (Halstead et al., 1977)

An early attempt at a generalized scheme was created by workers at Shell, (Halstead et al., 1971-1977), (Hirsch et al. 1976), and has been widely applied and validated (Griffiths, 1994). The Shell model requires calibration if a new fuel is used and the parameters are not directly linked to rate constants, but are empirically derived from rapid compression machine, RCM, results for ignition delay (Halstead et al., 1975). The scheme comprises the species RH, which is the initial fuel, the radical concentration R, the branching intermediate B, and Q, which is associated with an intermediate which can be formed in a cool flame and which is more prone to the abstraction of hydrogen atoms than the fuel.

The scheme uses a kinetic chain, which can propagate via the radical, R, via reactions 1 and 2. The branching agent, B, is formed in reactions 3 and 8, and causes branching in reaction 7. The initial chain may also produce the intermediate species, Q, in reaction 4, which can further react with R in a high temperature reaction pathway at increased rate compared to that of the parent fuel in reaction 8.

Because of the empirical nature of the Shell model, it can be adapted to a number of fuels and is capable of reproducing many combustion phenomena (Bradley, 1997). However, its generic form means that it is a poor representation of real combustion chemistry, and despite being capable of application to different fuels, it is not a trivial task to do so.

The Shell model was further developed by Cox and Cole (1985) who produced a more detailed reaction scheme, comprising 9 intermediate species and 18 reactions. The larger model produces results that fit experimental data equally as well as the shell model, but with improved parametrization and less need for calibration. The model reformulates the shell model in terms of more fundamental chemistry using generalised species groups: OH, R, RO_2, QOOH, OOQOOH, HO_2, ROOH, H_2O_2, and RCHO. The NTC region is reproduced by means of a reversible $R + O_2 \leftrightarrow RO_2$ reaction. The Cox and Cole reaction scheme can be shown as:

$$RH + O_2 \rightarrow R + HO_2 \quad (5)$$

$$R + O_2 \rightarrow RO_2 \quad (6)$$

$$RO_2 \rightarrow R + O_2 \quad (7)$$

$$R + O_2 \rightarrow alkene + HO_2 \quad (8)$$

$$RO_2 \leftrightarrow QOOH \quad (9)$$

$$QOOH \rightarrow alkene + RCHO + OH \quad (10)$$

$$QOOH \rightarrow cyclic\ ether + OH \quad (11)$$

$$QOOH + O_2 \leftrightarrow O_2QOOH \quad (12)$$

$$O_2QOOH \rightarrow RO_2H + OH \quad (13)$$

$$RO_2H \rightarrow R + OH \quad (14)$$

$$RH + OH \rightarrow R + H_2O \quad (15)$$

$$R + R \rightarrow RH \quad (16)$$

$$RO_2 + RCHO \rightarrow RO_2H + R \quad (17)$$

$$HO_2 + RCHO \rightarrow H_2O_2 + R \quad (18)$$

$$HO_2 + HO_2 \rightarrow H_2O_2 + O_2 \quad (19)$$

$$H_2O_2 + M \rightarrow 2OH + M \quad (20)$$

The Cox and Cole model, similarly to the Shell model, suffers with heat release rate problems (Griffiths, 1994) whereby the total heat release for reaction may be correct, but the release rate is too dependent on specific sections of the chemistry to be accurate through the entirety of reaction. This can pose problems when studying a phenomena occurring on shorter timescales than ignition delay, such as detonation, where a very rapid and very brief heat release is an important factor.

Hu and Keck (1987) further developed the model from Cox and Cole's efforts

The Hu and Keck scheme comprises 12 intermediate species and in addition to the Cox and Cole scheme, HO_2 intermediate reaction may now occur with the fuel. In addition, enthalpy change is used to calculate heat release for each reaction, adding considerably to its complexity. These efforts are reviewed by Griffiths (1994) who identified that while the levels of detail made the models more applicable to results obtained experimentally, the complexity of the model also made their application in computational fluid dynamics unrealistic at the time. This is because the computational cost of the scheme increases rapidly with increases number of species. Advances in computing might make the model feasible now, if not desirable.

Muller and Peters (1992) took a different approach, instead reducing complexity while attempting to maintain the accuracy of the model. This model, while simpler and more attractive to application in fluid dynamics, does not retain the negative temperature coefficient often observed in ignition delay profiles (Griffiths, 1994).

The Schreiber et al. (1995) reduced thermokinetic scheme is a five reaction scheme which models the auto-ignition based on the primary reference fuels (PRFs) i-octane and n-heptane. The model was developed in response to previous models, which had neglected the high temperature reactions in favour of the low temperature reactions important to ignition delay. Previous models, such as that of Muller et al. (1992), also improperly represented the negative dependency of ignition delay on temperature that is shown experimentally. The Schreiber et al. (1995) scheme includes chemical autocatalysis, which allows the negative temperature coefficient (NTC) of ignition delay to be reproduced. The model is simplified as far as possible, while maintaining the important qualitative features of the reaction, allowing the model's application within computational fluid dynamics.

1.6 Thesis Outline

Initially in Chapter 2, auto-ignition modelling with a reduced model will be approached. The next chapter will introduce a modified version of Schreiber et al. (1995) reduced model that has been developed for different fuels. Initially the model will be applied to i-Octane, and the results discussed. An attempt to obtain excitation time is made with the model and compared to the data of Peters et al. (2013).

In Chapter 3, the reduced model will be applied to two further fuels with the aim of eventually developing reduced modelling of excitation time to a reasonable degree.

In Chapter 4, the detonation diagram of Bradley et al. (2002) is discussed and developed. The diagram is shown to be more generally applicable than the narrow range of conditions previously computed had suggested. Further to the developing detonation boundary, a further deflagration boundary is added to the diagram.

Chapter 5 will discuss the application of the diagram to both fuels and engines. Fuels that have desirable anti-knock properties are identified.

Chapter 6 presents the dimensionless diagram of Mansour et al (2008), now developed to be complimentary to the ξ/ε approach, and allowing the assessment of fuels and engines in both laminar and turbulent burning regimes.

Chapter 7 will discuss the conclusions of this thesis and areas remaining where future work would be beneficial.

2 Reduced Thermokinetic Model

2.1 Introduction

The complex nature of combustion reactions of even simple fuels leaves some details of the reaction beyond the scope of current experimental methods. To attempt to resolve these details, one available option is numerical modelling. Fully detailed models are complete representations of all of the reactions that make up a combustion reaction, but are consequently very large and complex. A reduced model mimics the macroscopic behaviour of the reaction, grouping components and radicals together to form new species, which are representative of collections of species in the detailed model that show similar behaviour. This simplification of the chemistry while maintaining the essential behaviour of the reactions allows for a more compact model that can be adaptable to differing fuels and implemented in a wider range of contexts with vastly reduced computational cost.

This section introduces and assesses the reduced model implemented and adapted to these needs.

2.2 Modelling Requirements

The model is intended for application in internal combustion engines, in which mild auto-ignition may be the intended mode of reaction or, an unintended consequence, as in engine knock. In both instances, data on auto-ignition delay times are required for different fuels over a wide range of temperature and pressure. As an example, and because of its practical relevancy, the mathematical model will initially be applied to the primary reference fuels, *i*-octane/air and *n*-heptane/air including their blends.

However, it is desirable that the mathematical model should be able also to predict auto-ignition delay times for other fuels such as toluene, which is commonly used as an alternative reference fuel and surrogate for the high content of aromatics in gasoline fuels with anti-knock characteristics. The recent use of bio-ethanol as a fuel additive, or in some cases as a near-pure fuel highlights the need for the mathematical model to be able to adapt to a variety of differing fuels.

Paraffins such as *n*-heptane and *i*-octane commonly display a temperature range in which ignition delay times, atypically, increase with temperature, in a limited range of negative temperature coefficient, NTC. This creates a more exacting requirement of the model. In contrast, toluene does not have an appreciable NTC, so the model must be flexible.

The initial applications for the model are zero dimensional, with no spatial grid. The reactive charge mixture is assumed homogeneous, and contained within a core in which adiabatic changes might occur due to changes in volume and pressure. This assumption avoids the complexity of computation over a spatial dimensional grid. Non-homogeneous hot spot auto-ignition however, would require more detailed 2D or 3D CFD modelling. Detailed models can comprise very many species and hundreds, or even thousands of reactions for practical fuels. This makes their direct combination with 3D CFD prohibitive, as the full set of hundreds of reactions, comprising hundreds of species variables must be solved for each node in the mesh. For these reasons and the need for rapid explorative studies, reduced models, over generalised reaction pathways, are computationally less expensive and more suited to application in CFD.

2.3 The Mathematical Model

For present purposes, it is convenient to recognise two chemical kinetic regimes. The first is one of high temperature, exceeding about 1000K, while the other is below this threshold.

The kinetically generalised model is based upon that of Griffiths (Schreiber et al. 1994) because of its compact size, good adherence to phenomena such as the NTC region and its ability to be adapted simply to new applications (Bourdon et al., 2004). The present scheme lacks the Research Octane Number, RON, scaling factors of the original to allow adaptation to individual fuels. These scaling factors were applied by Schreiber et al. (1994) as a means to generalise the scheme. The Schreiber et al. (1994) correction factors take the form C= (110-ON)/10. In the original work of Schreiber et al. (1994), the forward component of reaction *3* is multiplied by C while reaction 4 is multiplied by $\sqrt{C}$. This serves as an interpolation between their reaction parameters for *i*-Octane and those for *n*-Heptane. Ideally this would allow any fuel with ON<110 to be simulated without calibration. However, as has already been discussed in Ch. 1, the ON systems are not applicable over a wide range of conditions. The maximum ON is also problematic for fuels such as ethanol, which exceed this threshold. Therefore, these correction factors are omitted from the present model.

The present scheme is outlined in Table 2.1. It comprises five reaction pathways (each with a rate constant) with six reactive species. Rather than take the Schreiber et al. approach to generalisation with RON, the model must be adjusted for differing fuels by directly adjusting reaction rate constants. This more general approach was taken for all fuels, with no use of RON.

Reaction Number	Reaction	Reaction Description
1 *High Temperature*	$F \rightarrow X$	Breakdown of fuel into branching intermediates
2 *High Temperature*	$X + aO_2 \rightarrow P$	Reaction of intermediates with oxygen to form products
3 *Low Temperature*	$F + 2O_2 \leftrightarrow I$	Reversible reaction converting between fuel and oxygen, and radical intermediate species
4 *Low Temperature*	$I \rightarrow 2Y$	Radicals react to form chain propagating intermediates
5 *Low Temperature*	$Y + 0.5F + (a\text{-}1)O_2 \rightarrow P$	Intermediates, fuel and oxygen react to form products.

Table 2.1 Reduced Reaction Scheme. F: fuel, O_2: oxygen, P: product, Y: chain propagating species, X: chain branching species, I: product oxygenated radicals.

Species *F*, O_2 and *P* are those of fuel, oxygen and grouped products respectively. *I*, *X* and *Y* denote intermediates. *a* is a numerical coefficient determined by the required oxygen. For stoichiometric *n*-heptane *a*=11, while for stoichiometric *i*-octane, *a*=12.5. Of these, *I* represents the product of low temperature regime oxidisation of the fuel to produce radical intermediates. *Y*, the chain propagating species, are then formed from *I* and react with fuel, *F* and oxygen to produce the products, *P*. In the high temperature chemical kinetic regime, *X*, the chain branching species, form from the breakdown of the fuel, *F*. The chain branching species, X, is then oxidised in Reaction *2* to form the products, *P*. Schreiber et al. (1994) gave the example of *i*-octane, where, in the low

temperature regime, the addition of two oxygen molecules to *i*-octane and loss of one water molecule leaves *I*, which in this case is the free radical $OC_8H_{15}O_2H$. *I* then breaks down into smaller chain propagating species, represented by *Y*. These chain propagating species may be thought of as OH, but should include other components, such as partially oxygenated products if chemical or enthalpy equilibrium is a concern. In the case of the high temperature chemical kinetic regime, oxidation of the *i*-octane produces chain branching intermediates, *X*. These intermediates are composed of such molecules as $3C_2H_4$, CH_2, CH_3, and also H.

Reactions *1* and *2* are the high temperature chain branching pathways proposed in the model of Muller, Peters and Lian (1992). Reactions *3*, *4* and *5* are the low temperature chain propagation pathways with lower activation energies developed by Griffiths (Schreiber et al. 1994). The reverse of reaction *3*, which is denoted as 3_R, acts almost as a switch between the two regimes of temperature. The two sets of equations, high temperature and low temperature, must each have identical overall enthalpies, in accordance with Hess's law, which states that enthalpy change when converting reactants to products is the same regardless of the path taken.

The NTC region is controlled within the low temperature reaction set by Reactions 3_R and *4*, which are competitive. Reaction *4* is able to take place at low temperatures, forcing the reactants to take the chain propagating path through Reaction *5*. At higher temperatures the higher activation energy of Reaction 3_R allows it to push the reactants back towards Reactions *1* and *2*, the chain branching pathways. The reverse reaction progresses much more quickly, reversing the formation of the intermediate *Y*, which is required for the low temperature oxygenation, Reaction *5*.

Reaction rates are assessed to be in Arrhenius form with a rate constant given by $k_n = Aexp-(E/RT)$, where n is reaction number. The constants for A and E/R used to calculate rate constants for *i*-octane as in Schreiber et al. (1994) are given in Table 2.

Reaction Rate Constant	A (mol m^3 s)	E/R (K)
k_1	5.10^8	18050
k_2	7.10^6	7200
k_3	$3.5.19^8$	19500
k_{3R}	6.10^{27}	37500
k_4	6.10^7	5000
k_5	1.10^9	16500

Table 2.2 Calculation of reaction rate constants for i-octane from Schreiber et al. (1994).

Schreiber et al. (1994) express the reaction rates as:

$$R_1 = k_1[F] \quad (1)$$

$$R_2 = k_2[X][O_2][M] \quad (2)$$

$$R_3 = k_3[F][O_2][M] \quad (3)$$

$$R_{3R} = k_{3R}[I] \quad (4)$$

$$R_4 = k_4[I] \quad (5)$$

$$R_5 = k_5[O_2][Y] \quad (6)$$

Where square brackets indicate species concentration (mol/m^3). From these reaction rates, the overall rate equation for each species is obtained by collecting all reactions containing that species. Reactions where the species is a reactant are

given a negative value, as the species is consumed, while reactions that have the species as a product have a positive value, as the species is produced. For example, the species [F] appears in Reactions *1*, and *3*, and *5* as a reactant, and *3R* as a product, its overall rate equation is thus formed by -R_1-R_3+R_{3R}-R_5:

$$\frac{d[F]}{dt} = -k_1[F] - k_3[F][O_2][M] + k_{3R}[I] - 0.5\,k_5[O_2][Y] \tag{7}$$

$$\frac{d[O_2]}{dt} = -a\,k_2[O_2][X][M] - 2\,k_3[F][O_2][M] + 2\,k_{3R}[I] - (a-1)k_5[O_2][Y] \tag{8}$$

$$\frac{d[Y]}{dt} = 2\,k_4[I] - k_5[O_2][Y] \tag{9}$$

$$\frac{d[I]}{dt} = k_3[F][O_2][M] - k_{3R}[I] \tag{10}$$

$$d\frac{[X]}{dt} = k_1[F] - k_2[O_2][X][M] \tag{11}$$

$$\frac{d[P]}{dt} = k_2[O_2][X][M] + k_5[O_2][Y] \tag{12}$$

Here $[M] = p/RT$ is the total concentration of all species.

Finally, the energy equation determines heat release and is therefore crucial to the rate at which the reaction progresses, this can be given as:

$$\frac{dE}{dt} = (H_1k_1[F]) - (H_2k_2[O_2][X][M]) - (H_3k_3[F][O_2][M]) - (H_{3r}k_{3R}[I]) - (H_4k_4[I]) - (H_5k_5[O_2][Y]) \tag{13}$$

Where H_n is enthalpy of reaction, obtained by Schreiber et al. (1994) as average values for *i*-octane such that the adiabatic flame temperature is reached at the end of reaction.

2.4 Solution of the model

The initial values required by the program are those of temperature, *T*, pressure, *P*, species concentration for each of the reaction kinetics species and nitrogen, N_2, and specific heat, c_p of the air/fuel mixture. The reaction is then calculated for one time step, and the energy equation used to determine change in pressure and temperature for the next time step.

Solutions of the reduced model were obtained using the built in ordinary differential equation solvers of Matlab. The chosen solver was ODE15s, designed for stiff problems. ODE15s is a variable order, multi-step solver based on numerical differentiation formulas. Parameters such as solution tolerance are set in the Matlab function *odeset*, which builds a structure array to control the ODE solver. ODE15s does not require discretisation by the user, instead the differential equations are entered into a function along with any calculations that need to be repeated for each time step. This includes the temperature dependant reaction rate constants, k_n, which are calculated at each time step. Values for the pre-exponential factor, *A*, and *E/R* are defined for each reaction equation in this function for the calculation of the reaction rate constants.

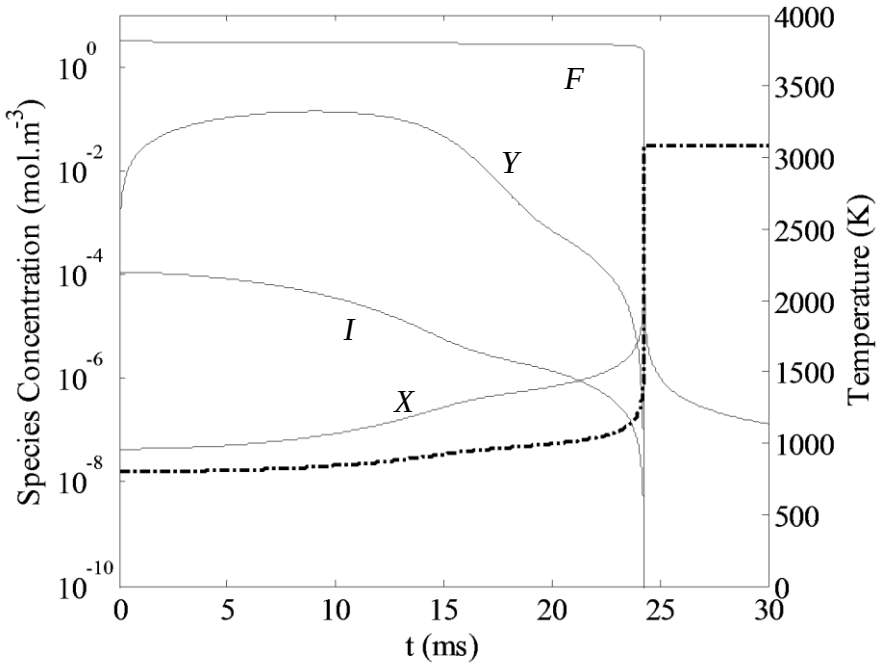

Figure 2.1 Species and temperature history for iso-Octane auto-ignition with initial temperature of 800K and initial pressure of 13bar.

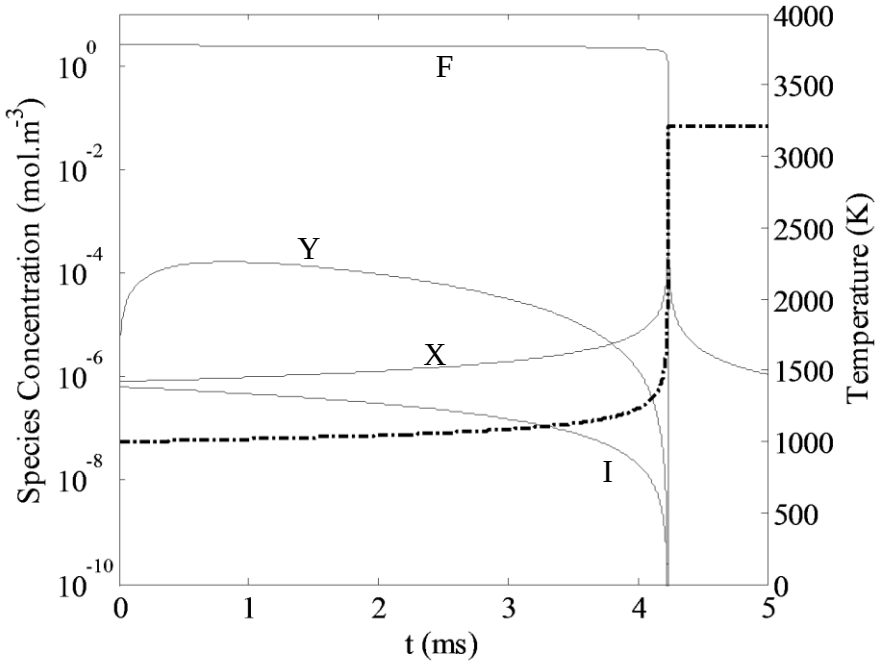

Figure 2.2 Species history for iso-Octane auto-ignition with initial temperature of 1000K and initial pressure of 13bar.

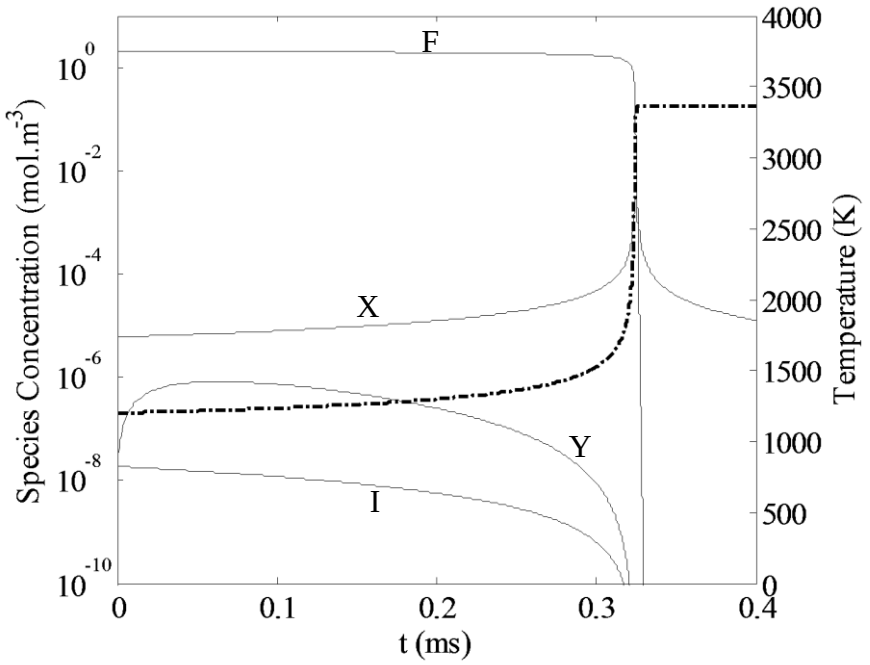

Figure 2.3 Species history for iso-Octane auto-ignition with initial temperature of 1200K and initial pressure of 13 bar.

The species concentration histories resulting from the solution of the reaction ODEs are plotted, as in Fig. 2.1. These give quite a clear indication of ignition delay time due to the sudden rapid change in fuel concentration. Figs. 2.1, 2.2 and 2.3 show only Fuel and intermediate species, as these are the most useful in both illustration and interpretation of the result. The chosen pressure was 13 bar, chosen for proximity to engine relative conditions and availability of corroborating data.

At initial temperatures less than 1000K, the *I* and *Y* intermediate groups, which are part of the low temperature pathway formed by reactions 2, 4 and 5, is clearly influential during the pre-ignition period. The propagating intermediates reach a peak concentration several orders of magnitude higher than that of the high temperature pathway branching intermediates, *X*. Closer to the point of ignition, when temperatures

have increased, concentrations of *X* start to increase, peaking steeply at the point of ignition.

The species concentrations in Fig. 2.1 show a transition between the low temperature chemical kinetic regime, and the high temperature regime. In this section of the plot, between about 12 and 23 ms, temperature is increasing through the 1000K transition between regimes and the otherwise smooth curves of the species concentrations show a small dip, in the case of *I* and *Y*, or a small peak in the case of *X*.

The concentrations of the intermediates are several orders of magnitude smaller than the fuel species, *F*, making it almost constant through pre-ignition. The point of ignition is easily identifiable by the almost step change in fuel species concentration, both visually and programmatically.

At an initial temperature of 1000K, any dominance of either pathway is less apparent. Here *Y* is most prevalent during pre-ignition, but the high temperature intermediate group *X* is still present in higher concentrations than the other low temperature group, *I.* At this temperature, the transition between low and high temperature regimes is being made in the rate equations. Both pathways are almost equally represented. The high temperature pathway that includes reactions 1 and 2 becomes more dominant as temperatures increase, with the branching intermediate species *X* showing an increasing concentration, while *Y* and *I* have decreasing concentrations.

The high temperature intermediate group, *X* has clearly now assumed a dominant role with the initial temperature of 1200K, being present in higher concentrations than either of the low temperature groups throughout the reaction and showing a positive gradient throughout the reaction period. Due to the short timescale of this reaction and therefore rapidly changing species concentrations, initial solutions showed instability.

In order to maintain stability for very short time scales, the solution array relative tolerance had to be tightened to 10^{-9}. In order to avoid the automatic time-step generation in the solver, which resulted in an excessively coarse time step, a time step is manually defined with the desired step size. This allows phenomena, which occur on a shorter timescale than the ignition delay itself to observed, while the automatically generated, coarse time stepping was inadequate even for ignition to occur in some cases.

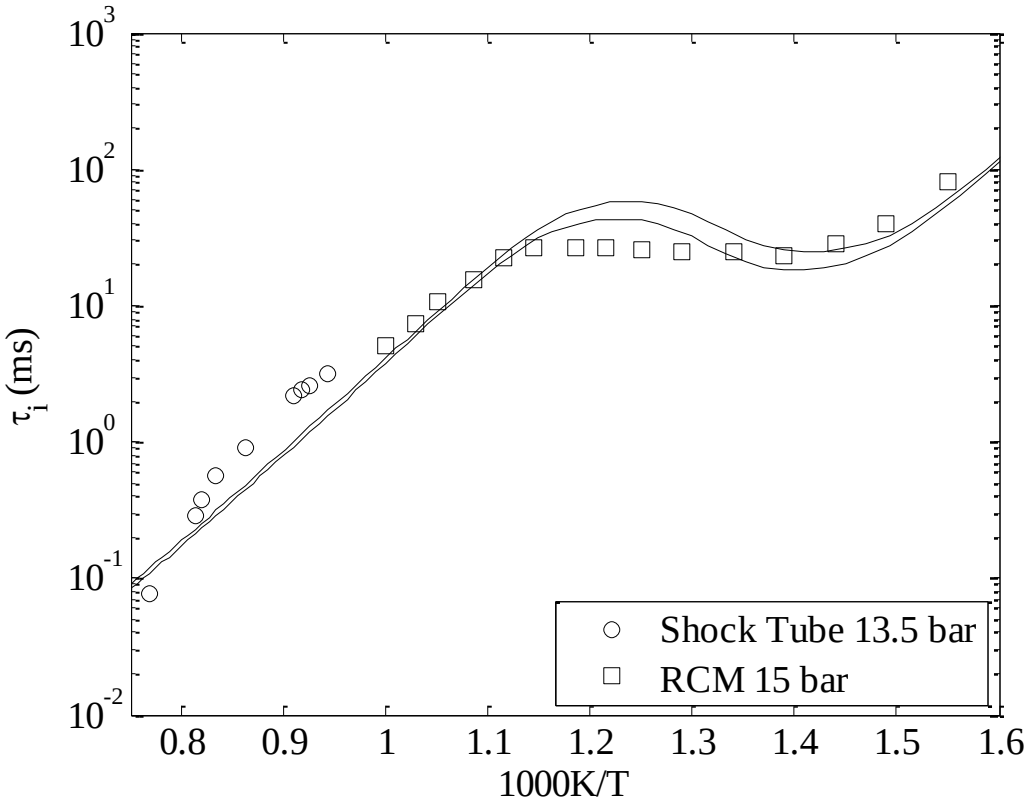

Figure 2.4 Arrhenius plot of stoichiometric i-Octane ignition delays with data from the shock tube study of Adomeit and Fieweger (1997) and RCM study of Voinov and Skorodelov (1965). Results of the reduced thermokinetic model are given in solid lines here showing pressures of 13.5 bar (upper) and 15 bar (lower).

Fig. 2.4 shows τ_i predictions of the reduced scheme compared with experimental data at 13.5 and 15 bar. At relatively low pressure the RCM study of Voinov et al (1965) provides experimental data for temperatures above 1000K while the shock tube study

of and Adomeit et al. (1997) provides data for lower temperatures. The model shows good general agreement with the shock tube data, only showing a more prominent NTC region. As temperature is increased above 1000K the agreement with the RCM data is not quite so good, with the model under estimating τ_i when compared with the experimental values.

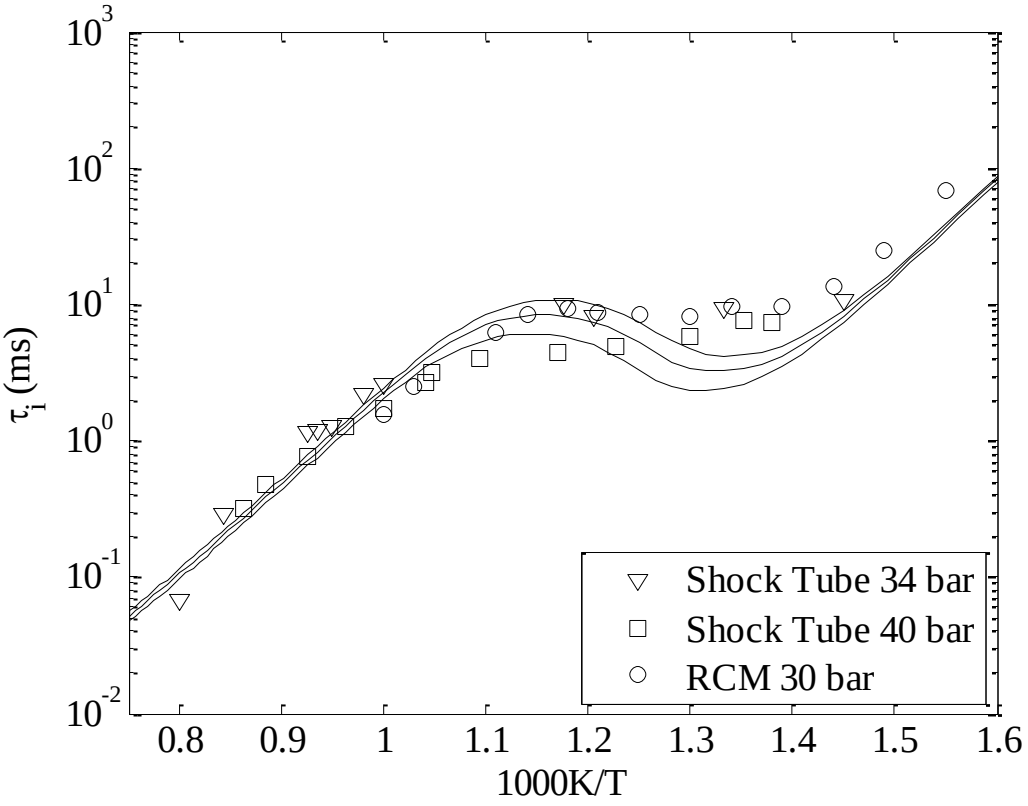

Figure 2.5 Arrhenius plot of stoichiometric i-Octane ignition delays with data from the shock tube study of Adomeit and Fieweger (1997) and RCM study of Voinov and Skorodelov (1965). Results of the reduced thermokinetic model are given in solid lines here showing pressures of 30 bar (upper), 34 bar and 40 bar (lower).

The results of the reduced model, when compared experimental data of Adomeit et al. (1997) and Voinov and Skorodelov (1965) at higher pressures in Fig. 2.5, gives a closer fit than those at lower pressure in Fig. 2.4. The agreement is reduced at temperatures lower than ~750K with the model again under estimating τ_i when

compared to the experimental data. In this region, however the longer ignition delay times make experimental measurement of τ_i increasingly susceptible to effects such as heat loss and reflected shocks, reducing their reliability.

The shock tube data shows only a minimal increase in ignition delay times in the NTC region, while the RCM results show a more pronounced effect. Both of the experimental data sets show a less prominent NTC region than that given by the reduced thermokinetic model, which has an almost sinusoidal appearance with a definite negative gradient through the NTC region.

2.5 Computing excitation time

Auto-ignition delay time, τ_i, may be defined as the period over which there is no heat release, terminated by an instantaneous heat release at the point of ignition. This seems like a reasonable definition based on experimental data, which seems to show exactly this except in the case of cool flame reactions. Computational studies with a sufficiently small time step, such as that by Lutz et al. (1988), show that in fact the heat release is not instantaneous but takes place over a finite amount of time, termed the excitation time, τ_e.

While auto-ignition delay time is relatively simple to obtain experimentally, current methods cannot provide accurate results for excitation time. This is not least because of the extremely short timescales involved but also because the reality of an experimental approach is initial reaction at a single point, or hot-spot, quickly followed by ignition at other points in the volume. This means that the observed excitation time in the volume is a much longer period than an individual excitation time. The only way to obtain excitation time data with current methods is therefore through numerical methods.

Thus far all existing τ_e data has been generated through the use of comprehensive modelling, making the use of a small time step computationally expensive, and prohibitive in applications such as CFD. Computation of τ_e within such an application may be attractive due to a significant role in detonation, discussed in Chapters 4 and 5. To that end, the reduced model will be applied to computing ignition delay reactions with a very small time step of 10^{-9} s. Initially this will be demonstrated here using the same configuration as above, but with a smaller time step of 10^{-9} s. Further calibrations and comparisons to existing data will be made in the following chapter.

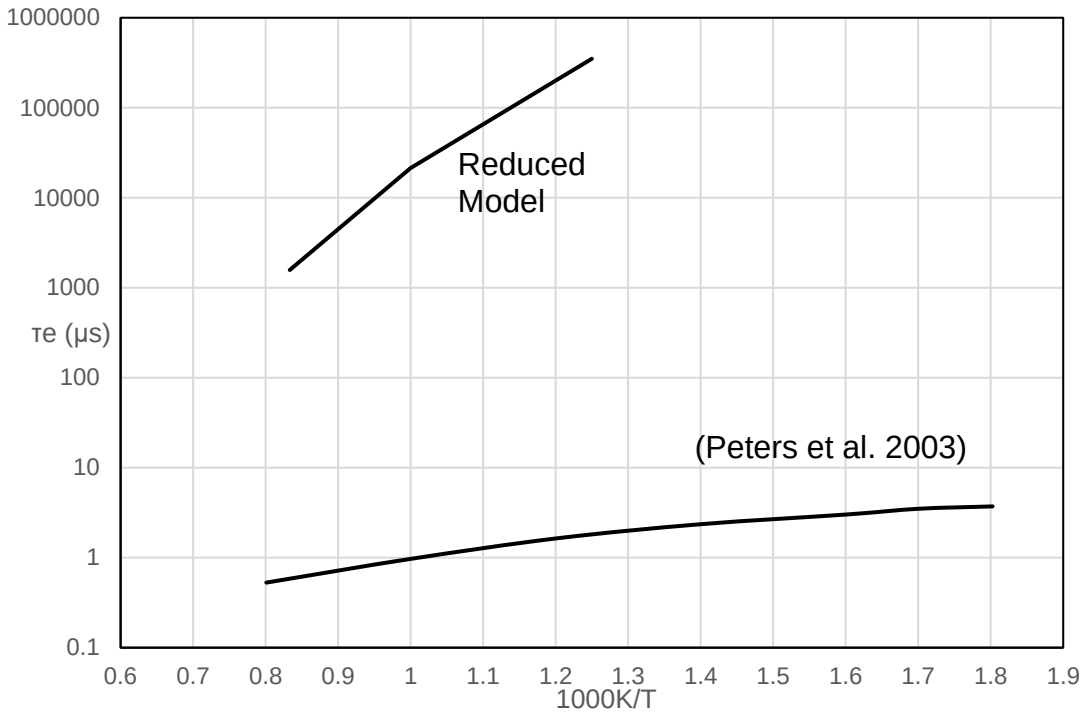

Figure 2.6: Excitation time generated by the reduced thermokinetic model for stoichiometric i-octane at 4 MPa compared to that of Peters et al. (2003).

The results of the reduced model are, for *i*-octane, disappointing with regard to excitation time. A difference of greater than three orders of magnitude and worse up to 6 orders of magnitude as temperature decreases. The following chapter will assess

the excitation time of simpler, faster reacting fuels, where the rate equations are more likely to correspond to those that are important in the excitation time, which share much higher heat release rates.

2.6 Conclusions

A reduced thermokinetic model has been introduced and developed to eliminate dependence on octane numbers. The model has been validated against ignition delay data for *i*-octane and a provisional attempt to simulate an accurate excitation time has been performed.

The model after removal of the octane number dependence should be able to replicate fuels that fall outside the range of *i*-octane and *n*-heptane mixtures.

The relative roles of the species and reactions encapsulated within the reduced model have been identified and the species histories analysed for a range of temperatures, which spans the transition between high and low temperature reaction sets.

3 Application of the reduced model

3.1 Introduction

The applications of computational models are widespread. Commonly reduced models are applied in engine models or in CFD. The application here is more what Griffiths (1995) terms a thought experiment: “Computation affords the opportunity to answer the question “What if . .?” regardless of whether or not that particular condition, or change of circumstances, is accessible by experiment.” The intention is to establish whether reduced modelling is an appropriate method for calculating excitation time, τ_e, a fuel property that is, at the current time, impossible to measure experimentally. As will be discussed in chapters 4 to 6, τ_e is an important factor in detonation. This implies that any attempt to model detonation in applications such as CFD should include calculation of τ_e. This is problematic because of the complexity of comprehensive models used for this computation. More desirable would be a reduced model, which can capture the relatively slow chemistry of the auto-ignition delay period, but also the very rapid chemistry of τ_e.

Even without the added computational cost of CFD, a reduced model may be desirable due to the very small time step needed to capture τ_e with any accuracy. τ_e operates on a timescale of µs, rather than the ms timescales of more commonly computed τ_i, requiring much smaller time steps for an equivalent resolution. The comprehensive mechanism for CH_4 used in this chapter required a time step of just 10^{-12} s to 10^{-14} s, for example.

The reduced model is applied to gauge the viability of this proposition. The scheme is calibrated to the τ_i produced by the respective comprehensive model at a temperature,

T, of 1000K at an appropriate pressure, *P*, before the time step is decreased in the region of rapid heat release.

3.2 Methane

Methane, CH_4, was among the first fuels simulated with sufficiently small time step to capture τ_e by Lutz et al (1988). The original computations simulated atmospheric pressure and relatively limited range of temperatures. The comprehensive scheme used has since been updated and improved by Smith et al. (1999). This updated scheme, GRI-Mech3.0 was used by Gorbatenko (2016) to first repeat the original conditions, and then extend their range to more practical conditions. The scheme comprises 325 elementary chemical reactions, with related reaction rate constants and the thermodynamic parameters of 53 species. This contrasts with the 7 species and 5 reactions computed in the reduced model presented previously (Schreiber et al. 1994).

GRI-Mech3.0 (Smith et al. 1999) has improved kinetics and broader target data compared to previous versions of this mechanism and has been validated against variety of experimental data for methane and natural gas based on flame speeds and shock tube measurements between 1000-2500 K and pressures between of 0.001 and 1.01 MPa by Huang et al (2004).

The reduced mechanism is calibrated manually by altering reaction rate parameters while maintaining overall heat release and ensuring that Hess's law is obeyed and both the high and low temperature pathways have equal heat release. Values are chosen to provide optimal results when compared to the detailed model for stoichiometric methane at a pressure of 6 MPa and temperature of 1000K. The resulting model

parameters are shown in Table 3.1, which also includes enthalpy of reaction, H_0, which is used in the energy equation. The reduced model remains applicable within a range of about 3 MPa and between 850K and 1300K. Better agreement at low pressures could be achieved with a second set of model parameters, but a second calibration has not been performed in this case.

Rate Constant	A (mol m^3 s)	E/R (K)	H_0 (kJ/mol)
k_1	6.10^7	18050	4.10^5
k_2	4.10^7	7200	$-7.5.10^5$
k_3	3.10^6	20000	-4.10^4
k_{3R}	3.10^{23}	37500	-4.10^4
k_4	2.10^7	5000	-6.10^4
k_5	6.10^7	16500	-3.10^5

Table 3.1: Reaction rate controlling parameters for the reduced model for CH_4.

The reduced and comprehensive scheme results are compared in Figs. 3.1, 3.2 and 3.3 with values of τ_i for stoichiometric CH4/air at 4, 6 and 10 MPa respectively computed with both the reduced model and comprehensive scheme. Comprehensive modelling results were provided by Gorbatenko (2016). The ratio of values of τ_i produced by each scheme at each pressure remains between 0.5 and 2 even where the curves deviate in the low temperature region. Within the region of best fit, the ratio is close to one, falling between 0.7 and 1.25.

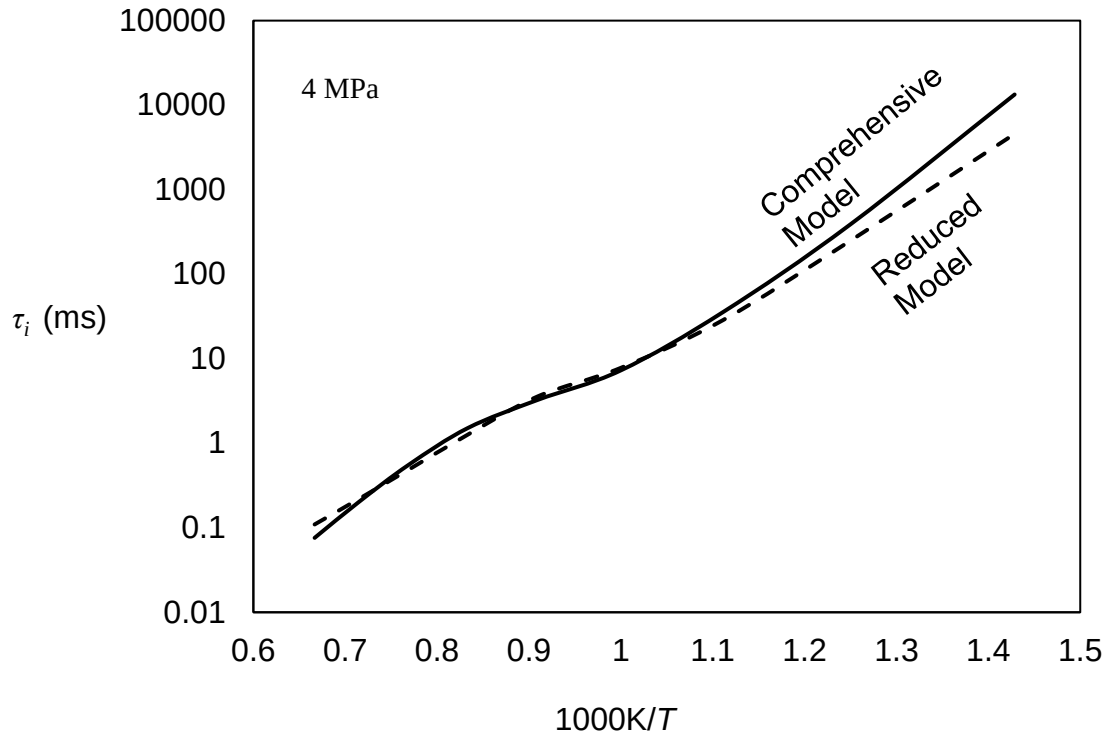

Figure 3.1: Comparison of ignition delay times predicted by Comprehensive and Reduced models for stoichiometric CH4/air at 4 MPa.

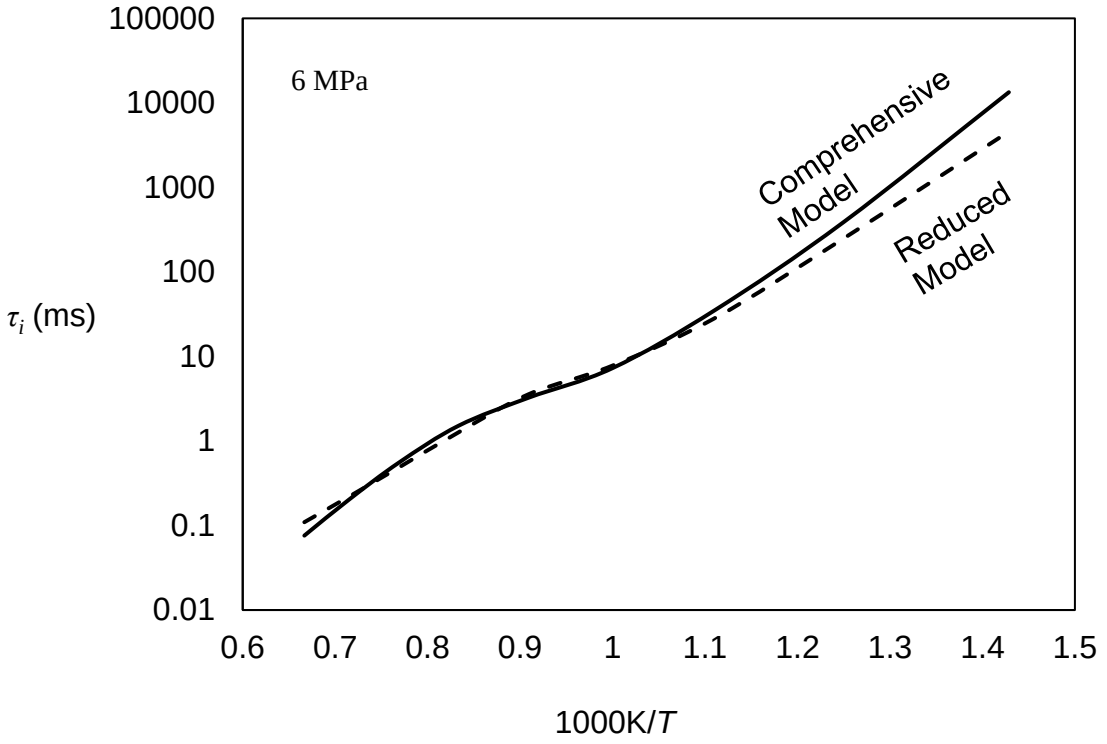

Figure 3.2: Comparison of ignition delay times predicted by Comprehensive (Gorbatenko, 2016) and Reduced models for stoichiometric CH4/air at 6 MPa.

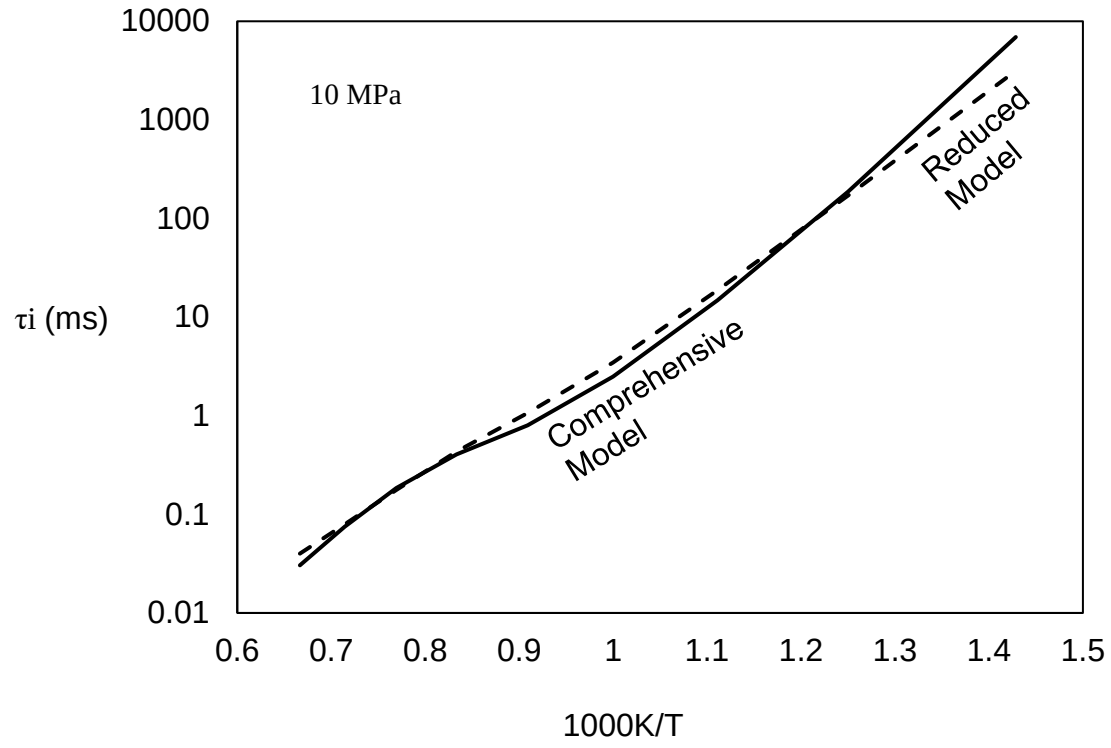

Figure 3.3: Comparison of ignition delay times predicted by Comprehensive (Gorbatenko, 2016) and Reduced models for stoichiometric CH4/air at 10 MPa.

Fig. 3.2, at 6 MPa shows the condition for which this calibration of the reduced model is best suited. While CH_4 does not show a true NTC region, there is a slowing in the region where one might be expected with other fuels, of around 1100K to 900K. For 6 MPa the reduced scheme is able to closely match the comprehensive results for ignition delay through most of the temperature range, including this region of reduced temperature coefficient. Only when the temperature, *T*, drops below about 800K is any significant deviation observed.

Excitation time data was computed using both the detailed and reduced thermokinetic models and the results at 4 MPa are compared in Fig. 3.4. Significant differences can be observed between the two data sets, with the reduced model results giving much

longer excitation times, two orders of magnitude greater than those of the comprehensive scheme even at conditions where good agreement is reached for τ_i.

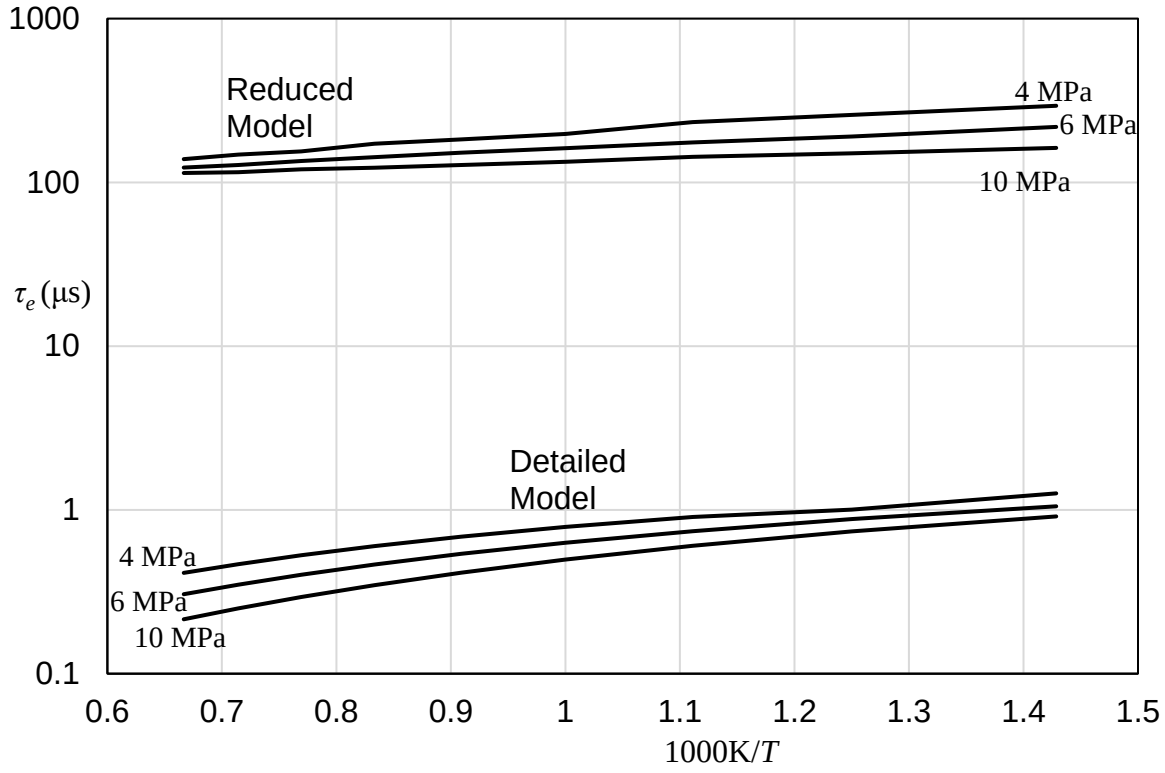

Figure 3.4: Comparison of excitation times generated by reduced and comprehensive (Gorbatenko, 2016) models for stoichiometric CH4 at 4, 6 and 10 MPa

Already implications for reduced modelling in applications such as engine models or in CFD are apparent. While the reduced model is sufficient to detect the presence of auto-ignition and to give the delay period, the period over which the bulk of heat release occurs is much longer than that of the detailed model, making accurate detonation modelling with the reduced scheme improbable.

The difference in heat release is large, but the general trends are similar. The reduced model tends to diverge between different pressures at the low temperature end, while

the comprehensive model is more parallel. Otherwise the two schemes share a gently decreasing gradient with temperature. Although the gradient appears to be proportional to their relative magnitudes on the logarithmic plot.

Although the single stage reduced global model, was able to generate sufficiently accurate values of $\tau_{i,}$ close to those of the comprehensive scheme, not surprisingly, the same cannot be said of the values of τ_e. Despite the employment of sufficiently small time increments in the computations of τ_e, the computed values, from the same global reaction parameters as for τ_i, were several orders of magnitude greater than those from the comprehensive scheme.

	Reaction Rate Constant	A (mol m^3 s)	E/R (K)	H_0 (kJ/mol)
τ_i	k_1	$2\cdot10^8$	19050	0.05
	k_2	$2\cdot10^8$	7200	-99
	k_3	$5\cdot10^6$	20000	-0.025
	k_{3R}	$6\cdot10^{21}$	37500	0.025
	k_4	$4\cdot10^6$	5000	-0.025
	k_5	$1\cdot10^7$	16500	-99
	Reaction Rate Constant	A (mol m^3 s)	E/R (K)	H_0 (kJ/mol)
τ_e	k_1	$1.05\cdot10^{10}$	21050	1000
	k_2	$1.05\cdot10^{10}$	8600	-10000
	k_3	$6\cdot10^9$	20000	-1000
	k_{3R}	$3\cdot10^{20}$	36500	1000
	k_4	$7\cdot10^9$	5000	1000
	k_5	$7\cdot10^9$	16500	-8000

Table 3.2 Reaction rate controlling parameters for Global Model G2.

The original intention of this particular global scheme was to facilitate the calculation of τ_i, including any regime of negative temperature coefficient, NTC, and these aims were achieved in the present study. However, it is in the nature of such a simulation that details of reactions on much shorter time scales are sacrificed. In an attempt to rectify some of these shortcomings of the reduced scheme, referred to as G1, and improve predictions of τ_e, an alternative approach was adopted in scheme G2. This employs two distinct sets of rate parameters and heats of reaction. The first set is to compute τ_i, the second to compute τ_e. Both sets of these G2 global parameter values are given in Table 3.2. The numerical values in the two sets are very different, as they are also when compared with those of the G1 scheme in Table 3.1. The two set approach necessitates much higher heats of reaction, H_0, for the computation of τ_e. In contrast, for the computation of τ_i heats of reaction were chosen to give very little heat release over the pre-ignition period, lower than those employed in the G1 scheme. This necessitates higher reaction rate parameters for the G2 scheme. The parameter sets are applied in such a way that during the pre-ignition phase, only the τ_i set is active, at the point of ignition the parameter sets immediately switch, so that now only the τ_e set is active. For both data sets the aims were to approach the predictions of τ_i, and τ_e given by the comprehensive scheme as closely as possible.

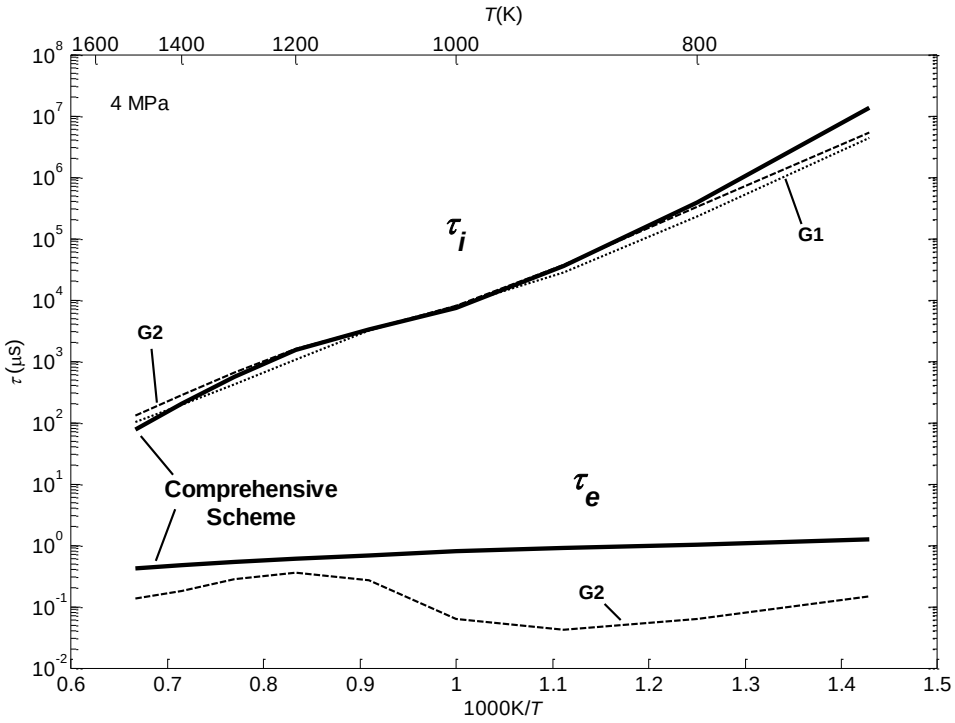

Figure 3.5 Comparison of ignition delay times, τ_i, and excitation times, τ_e, predicted by Comprehensive and Global schemes, G1 and G2, for stoichiometric CH4/air at 4 MPa.

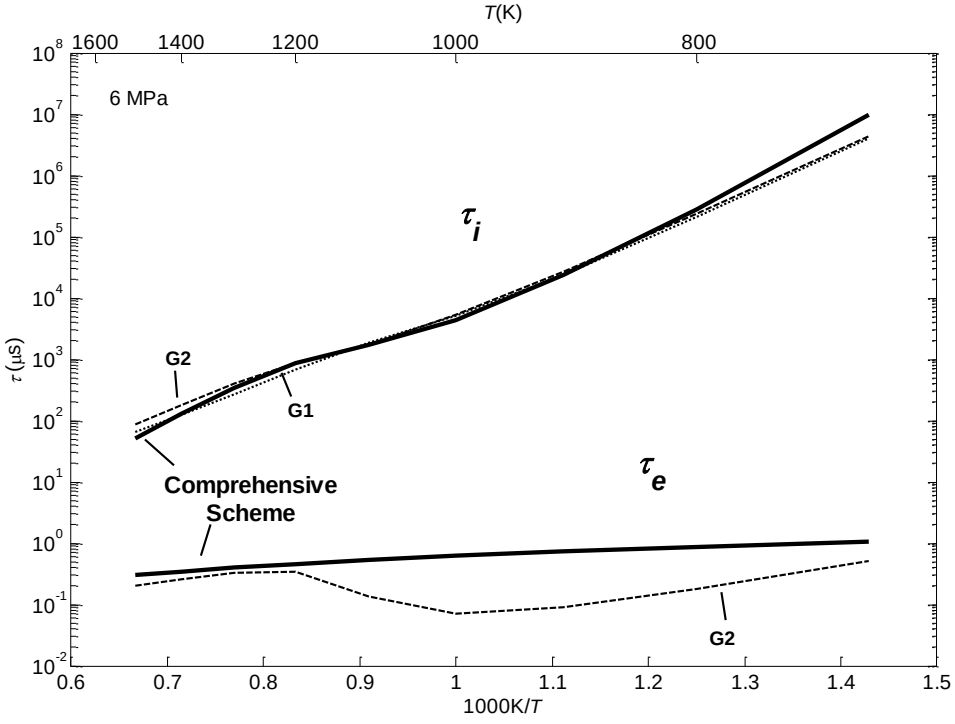

Figure 3.6 Comparison of ignition delay times, τ_i, and excitation times, τ_e, predicted by Comprehensive and Global schemes, G1 and G2, for stoichiometric CH_4/air at 6 MPa.

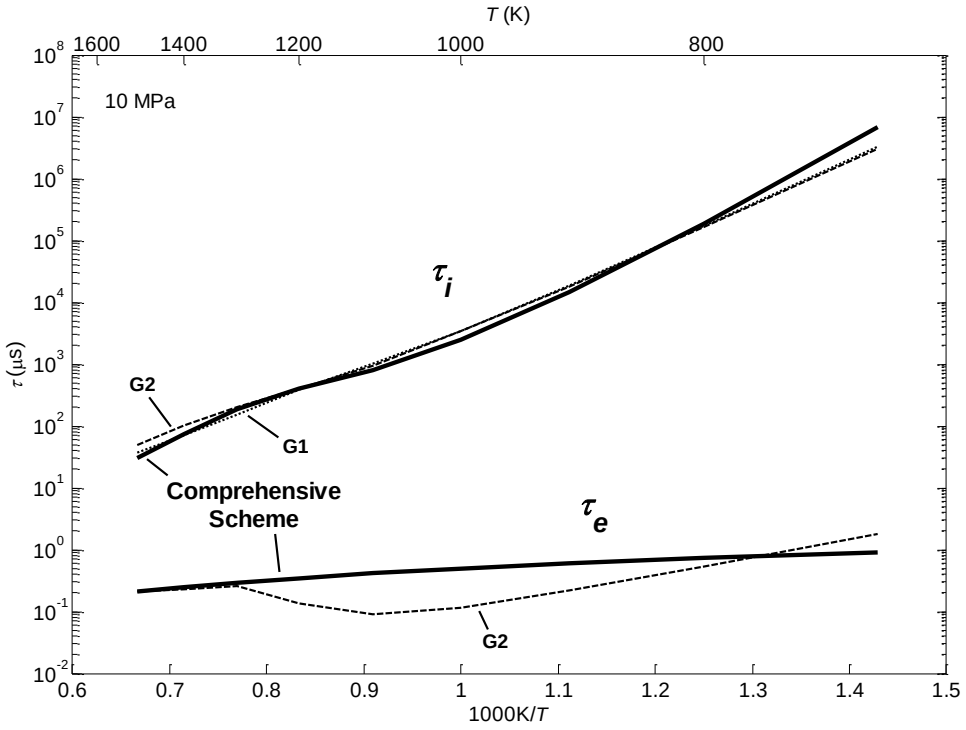

Figure 3.7 Comparison of ignition delay times, τ_i, and excitation times, τ_e, predicted by Comprehensive and Global schemes, G1 and G2, for stoichiometric CH_4/air at 10 MPa.

The resulting predictions using the G2 scheme are shown in Figs. 3.5 to 3.7. It can be seen that the G2 predictions of τ_i are close to those of the G1 scheme, but with a tendency to over-predict at the higher temperatures. Unlike the G1 scheme, the G2 scheme was capable of giving reasonable predictions of τ_e, although these were generally under-predicted by up to almost an order of magnitude. However, the general trend with varying temperature was to follow the predictions of the comprehensive scheme. The reduced scheme results exhibit an NTC region for τ_e, which is not present in the results from the comprehensive scheme. In Figs. 3.5 to 3.7 the temperature range of the NTC region is very similar for both τ_i and τ_e curves produced by the reduced scheme for a given pressure. The magnitude of the τ_e NTC region also appears to show proportionality to that of the τ_i NTC region.

The use of the same species for both τ_i and τ_e appears to have introduced an NTC region in the τ_e curves. Currently there is no transition between the two stages of the reaction, so remaining intermediate species from the pre-ignition stage are also present after ignition has occurred. As these species cannot simply be deleted, the heat release stage of the current scheme inherits some features from the pre-ignition stage, including the NTC region.

3.3 H_2/CO

The DNS study of Bradley et al. (2002) and Gu et al. (2003) used H_2/CO in an equi-molar mixture with air because of relatively well understood chemical kinetics, making it a good candidate to assess the capability of a reduced scheme to simulate excitation time. Fitting of the reduced scheme was again performed for a stoichiometric mixture at 1000K, available data necessitated that P=5 MPa. The resulting parameters and enthalpy of reaction, H_0, are given in Table 3.2.

Rate Constant	A (mol m^3 s)	E/R (K)	H_0 (kJ/mol)
k_1	6.10^9	21000	4.10^5
k_2	4.10^9	22000	$-7.5.10^5$
k_3	3.10^8	25000	-4.10^4
k_{3R}	3.10^{27}	37500	-4.10^4
k_4	2.10^6	8000	-6.10^4
k_5	6.10^9	16500	-3.10^5

Table 3.3: Reaction rate controlling parameters for the reduced model for H_2/CO.

The auto-ignition delay curve generated by these parameters is shown in Fig.3.5 and are compared to the original comprehensive mechanism results of Gu et al. (2003). The time step used required higher density because of the relatively rapid reaction, the ignition delay period was computed at a time step of 10^{-6} s, while the excitation period at a time step of 10^{-10} s.

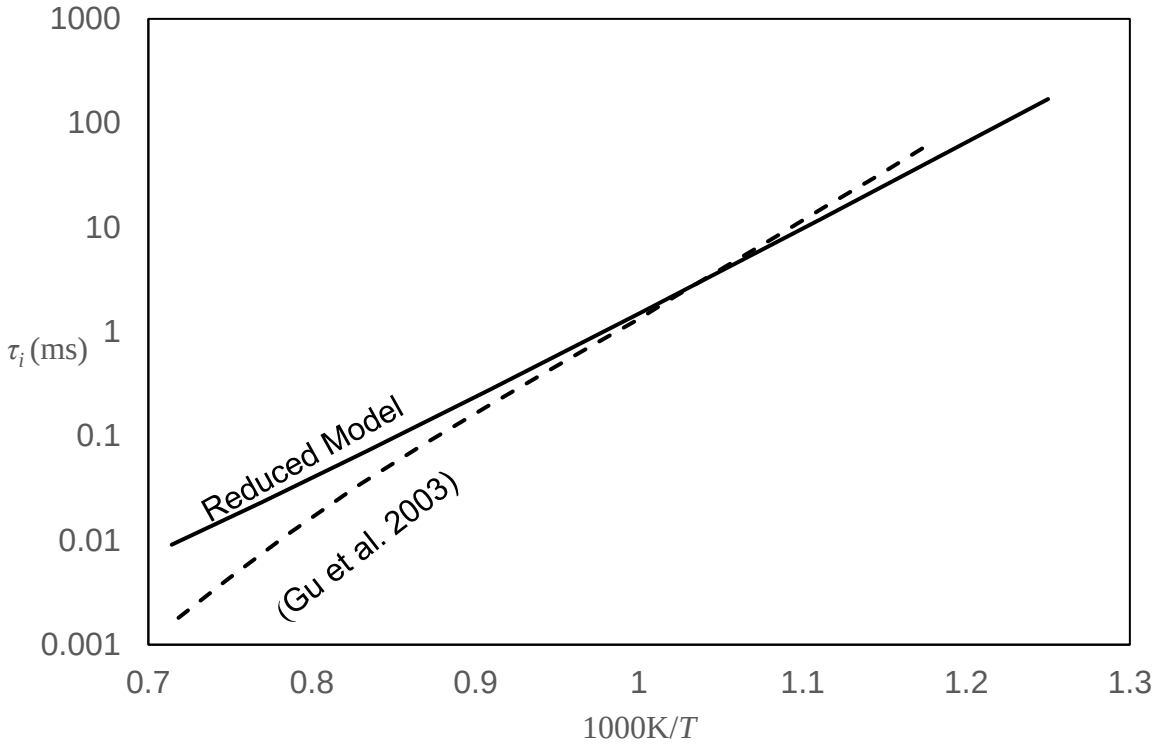

Figure 3.8: Auto-ignition delay of stoichiometric H2/CO equi-molar blend at 5 MPa

The general agreement in this case is not quite as good as that of the previous methane calibration, with Gu's data accelerating away from the reduced model result at the high temperature end of the diagram. The curves remain within a difference that might be expected of experimental scatter.

When the time step is decreased, however, there is again a large difference between comprehensive and reduced modelling results. This can be seen in Fig. 3.6, where the excitation curves of the two schemes are compared.

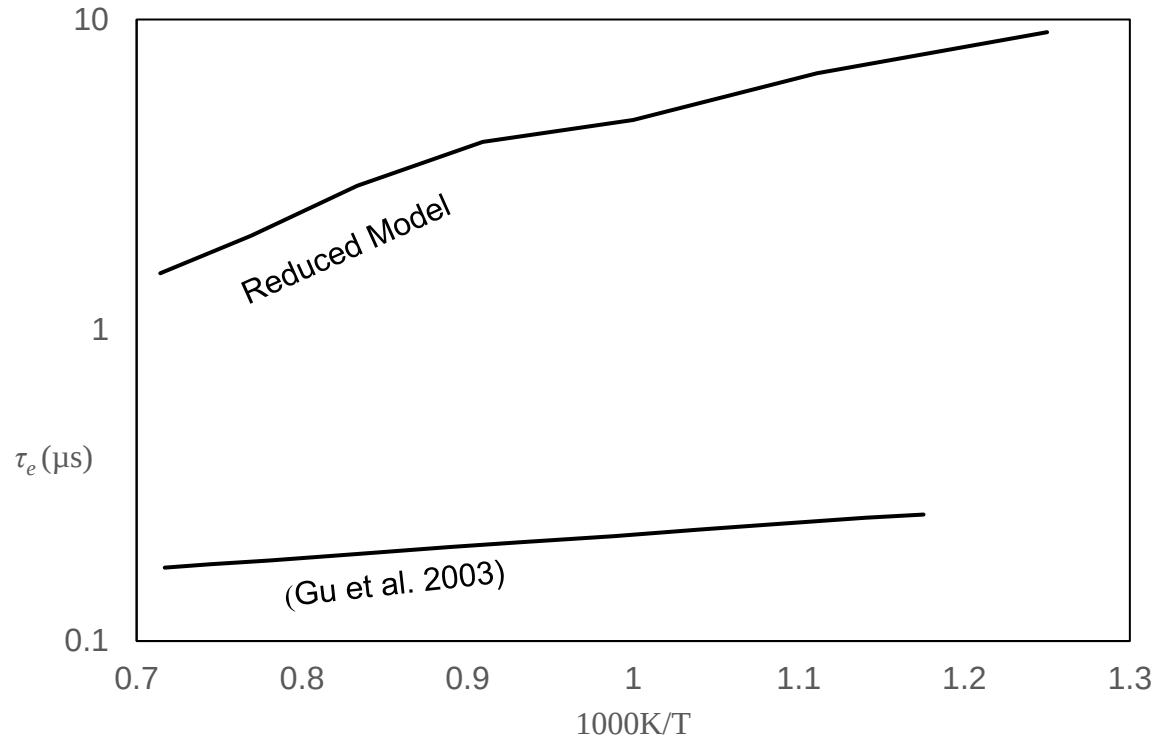

Figure 3.9: Comparison of excitation times generated by reduced and comprehensive mechanisms for stoichiometric H_2/CO at 5 MPa.

The difference between models is now less severe, with only about one order of magnitude discrepancy. This is obviously still inappropriate for direct application to detonation in CFD. The curves also differ in gradient, with the reduced model showing some non-linearity not experienced by the comprehensive model.

The large differences between comprehensive and reduced model results is indicative of differences in the governing chemistry of the excitation period compared with those of the ignition delay period. The reduced model does not have sufficient detail to encompass the chemical differences in the two periods. As a result the relatively slow

chemistry is also governing heat release after ignition. The heat release is prolonged and therefore prone to generate spurious results if implemented in the wrong context.

The minimum requirement for accurate simulation of excitation time appears to be a second, dedicated model, or at least a dedicated set of rate parameters specific to the excitation period.

3.4 Conclusion

The reduced model developed in the previous chapter has been successfully applied to simulation of auto-ignition delay time, τ_i, for two fuels very different to the original PRFs the model was intended for by Schreiber et al (1994).

The scheme was able to achieve good agreement with both CH_4 and H_2/CO τ_i data, but incapable of direct reproduction of excitation time based solely on the τ_i calibration.

Governing chemical reactions determining the rapid progression through the heat release region are determined to be sufficiently different to those that govern the ignition delay period to warrant the use of a separate model or rate parameters.

A two-stage reaction scheme was devised by duplicating the reaction set and assigning new reaction rate parameters to each stage. The two-stage scheme's rate parameters are chosen to reflect the very different heat release rates shown between the pre-ignition stage and the excitation period of the reaction. This preliminary two-stage scheme was able to outperform the previous single stage approach in predicting τ_e, whilst maintaining overall heat release and its ability to predict τ_i.

4 Propagation from a hot spot

4.1 Introduction

The octane rating systems, RON and MON, as well as variations of them to allow for contemporary fuels and engines, and alternate methods for characterisation are discussed in the introduction section of this thesis. All of the discussed methods are empirical in nature and, while they improve on RON and MON for contemporary engines, they share many of the same shortcomings. This chapter begins to address this by outlining a fundamental approach to characterisation of both fuels and engines, which removes problems introduced by empiricism.

Zel'dovich (1980) showed that a detonation must originate from an auto-ignitive hot spot and that the reactivity gradient across this hot spot is instrumental in the development of detonation. At a critical gradient for a given fuel and condition, the reaction front will progress at a rate similar to that of the sound speed of the mixture, leading to coupling of the reaction front with the pressure wave, acceleration of the coupled fronts to eventual detonation. Larger gradients might lead to more conventional propagation by deflagration or auto ignition, while very small gradients can result in supersonic reaction propagation with no coupling with the pressure wave, or a thermal explosion.

If coupling of the pressure wave and the reaction front does occur, the severity of the resulting developing detonation can range from a benign knock at sufficiently large temperature gradients, through severe knock, to super knock with sufficiently small temperature gradient. Severe knock may cause damage to an engine, while super

knock is defined as an overpressure 10 times that of a normal combustion cycle that is free of knock or detonation.

Characterisation of these phenomena is particularly important in internal combustion engines, where knock and detonation are limiting factors to efficiency. Avoiding these regimes while increasing compression ratio, and therefore *T* and *P* at TDC, creates more efficient engine operation. Other applications could include hazards; such as fuel storage or transport.

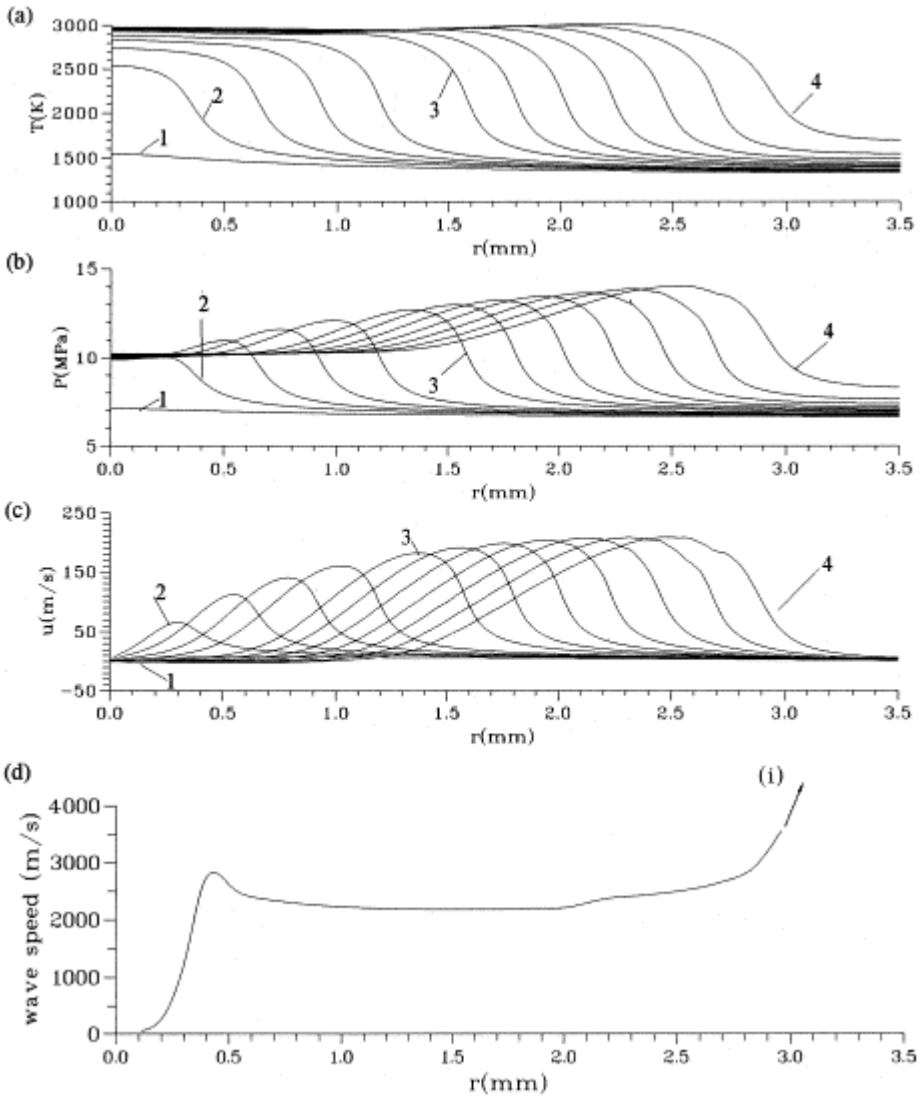

Figure 4.1: History of a hot spot, r_o = 3 mm, with ξ =1, stoichiometric 0.5 H_2/0.5 CO/air, T_o= 1200K and P_o=5.066 MPa, τ_i = 39.16 μs. Time sequence (μs) 1-35.81, 2-36.16, 3-36.64, 4-37.43, 5-37.72, 6-38.32, 7-38.86, 8-39.13. (a) temperature, (b) pressure, (c) combustion wave speed. (Gu et al. 2003)

Fig. 4.1 shows results from the DNS studies of Bradley et al. (2002) and Gu et al. (2003), for a detonation developing rapidly from a hot spot of radius 3 mm in a stoichiometric 0.5 H_2/0.5 CO/air mixture with ξ = 1.0 at 1200K, τ_i = 39.16 μs and a = 731 m/s.

Profile 1 in Fig. 4.1 (1.4175 ms) shows the start of reaction. Between profiles 1 and 2 (1.4185 ms) peak pressure increases to a point where the pressure wave is sufficiently developed to compress the unburned gas ahead of it. Between profiles 2 and 3 (1.4191 ms) the pressure wave couples with the reaction front, causing both to increase in magnitude. After profile 3 the coupled waves form an almost fully developed detonation. After profile 4 (1.4222 ms) the coupled waves have reached the outer edge of the hot spot as a detonation wave, which then rapidly accelerates to thermal explosion in the remainder of the combustion volume. The temperature gradient across the hot spot was -2.426 K/mm and the thermal diffusivity -0.564 μs/K, smaller in magnitude than the value of Meyer and Oppenheim. A hot spot developing to thermal explosion was also investigated by Bradley et al. (2002) and Gu et al. (2003) with φ = 0.75 and at 1000K, which showed thermal diffusivity of -32 μs/K.

Bradley et al. (2002) were able to identify through an laborious DNS study, the location of boundaries, ξ_u (upper) and ξ_l (lower) for stoichiometric 0.5 H2/0.5 CO/air mixtures in a narrow temperature band of 1000K to 1100K, the resulting peninsula diagram is shown in figure 4.2. Detonation can develop within the bounds of the peninsula, but not outside the boundaries.

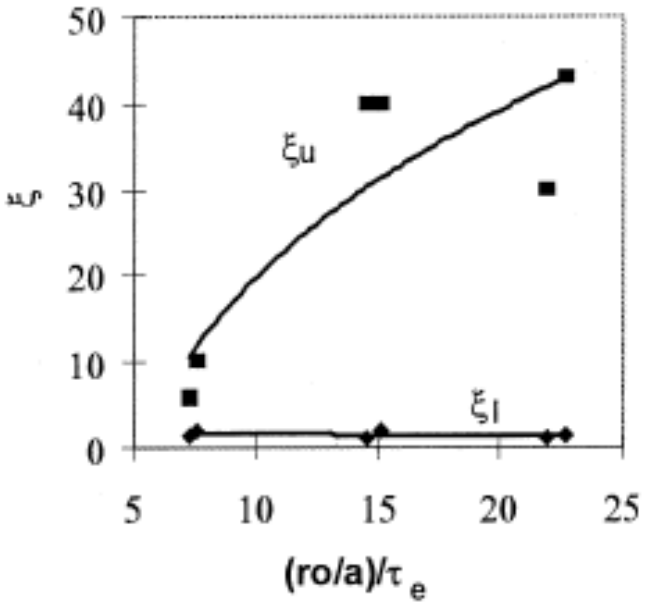

Figure 4.2: Detonation peninsula diagram for 0.5 H2/0.5 CO / air mixture (Bradley et al., 2002)

The purpose of this chapter is to further develop this approach and extend its capabilities to describe the behaviour of a reaction initiated from a hotspot for turbulent combustion regimes. The application of this approach will be covered in the following chapter.

4.2 Auto-ignition in a secondary hotspot

The phenomena leading to super-knock are a rather complex sequence of events comprising the primary formation of hot spots that pre-ignite and initiate premature flame propagation, with earlier increases in pressure and temperature in the unburned mixture. This may create a secondary, more reactive, hot spot in the reactants and lead to a developing detonation, following the theory developed by Bradley (2002) and Gu (2003). While the salient features of the latter appear to be understood, the mechanisms causing primary hot spots are still the subject of debate. Localised heating caused by

turbulent dissipation is not likely to be a factor due to the small quantity of energy involved (Bates et al. 2016), however turbulence may play a part in hot spot generation through small scale mixing of the reactants with recirculated exhaust gas. Hot spots might also be formed by heat transfer from hot surfaces, such as an exhaust valve, after a particularly high temperature cycle.

A type of knock that is specific to turbocharged direct injection engines is LSPI, Low Speed Pre-Ignition. This occurs with the engine at low speed and at high load condition (Andrews et al. 2016). Cyclic LSPI, with pre-ignition occurring on alternate cycles. is observed by Dahnz et al. (2010) and Dingle et al. (2014). This was attributed its cause to formation of mixed fuel-oil droplets which are both more prone to stripping from clinder walls than the lubricant oil and have reduced τ_i compared to the fuel. Cyclic behaviour is also observed by Kalghatgi & Bradley (2012); a severe engine cycle resulted in high exhaust *T* and *P*, and consequently little air inhalation in the following cycle. This cycle is then relatively cool, allowing increased air inhalation, and so generating another severe cycle. The effect of lubricant oil composition on LSPI is investigated by workers at Toyota (Fujimoto et al., 2014), (Takeuchi et al., 2012), and (Hirano et al., 2013) who identified a correlation between the auto-ignition temperature of lubricant oil and LSPI. Calcium, Ca, was found to be a lubricant oil additive that is a significant contributor to LSPI. Zahdeh et al. (2011) found that minimising the possibility of oil and fuel mixing, including by targetting injector spray, also minimised LSPI. Workers at GM (Sczomak et al., 2003) have developed a central location for fuel injection, which avoids piston liner wetting, but also compromises packaging, potentially requiring reduced valve sizes and so compromising performance. A more conventional side injection platform has been developed by workers at Toyota (Matsumura et al., 2013), with a fan shaped cross

section jet spray and injection angle optimised to match flow from the air intake valve. This system relies on high injection pressure and enhanced tumbling effect, referring to rotational fluid flow within the cylinder, to mix the fuel-air charge sufficiently and to minimise piston liner wetting.

The earlier the initial pre-igniton, the more severe is the secondary auto-ignition. The secondary hot spot which can potentially initiate a detonation is the now analyzed.

The auto-ignition delay time at a given pressure is expressed by:

$$\tau_i = Cexp\ (E/RT), \text{ and} \tag{1}$$

$$\partial\tau_i/\partial T = \tau_i(E/RT^2) \tag{2}$$

The localised activation temperature, *E/R*, is expressed by:

$$\partial \ln \tau_i/\partial(1/T) = E/R \tag{3}$$

Assuming that the fuel/air charge is otherwise homogeneous and that the reactivity gradient at the hotspot is due only to temperature gradient, the auto-ignition propagation velocity is

$$u_a = \partial r/\partial\tau_i = (\partial r/\partial T)(\partial T/\partial\tau_i) \tag{4}$$

Detonations are associated with the auto-ignitive front propagating at close to the acoustic velocity, a, and it is intuitive to introduce the dimensionless ratio ξ:

$$\xi = a/u_a = (\partial T/\partial r)(\partial\tau_i/\partial T) \tag{5}$$

A critical value of the temperature gradient, signified by suffix *c*, occurs when $\xi = 1.0$, and from Eq. (5),

$$(\partial T/\partial r)_c = (\partial T/a\partial\tau_i). \tag{6}$$

From Eqs. (5) and (6),

$$\xi = (\partial T/\partial r)(\partial T/\partial r)_c^{-1} \quad (7)$$

For a given mixture and its conditions, ξ is proportional to $\partial T/\partial r$.

From Eqs. (2) and (5), and considering the temperature gradient $\partial T/\partial r$ to be negative;

$$\xi = -\tau_i(E/RT^2)(\partial T/\partial r)a. \quad (8)$$

Both Voevodsky and Soloukhin (1965), and Meyer and Oppenheim (1971), employing H_2/O_2 mixtures, used Eq. (3) to define the boundary between strong and weak auto-ignitions. Strong ignition was defined as a stable detonation, with near-instantaneous and uniform auto-ignition, and a low value of the thermal diffusivity, $(\partial\tau_i/\partial T)$. Meyer and Oppenheim suggested a threshold value of $\partial\tau_i/\partial T$ for this regime of - 2 μs/K.

The other relevant dimensionless group, ε, is a measure of the amount of energy transferred to the acoustic pressure wave as it travels through the hot spot. The residence time of this wave is given by the dimensionless hot spot radius, r_o, divided by the acoustic speed. This residence time is then divided by the excitation time, τ_e, which is the period during which the majority of heat release takes place in an auto-ignition. This gives the dimensionless group ε:

$$\varepsilon = r_o/a\tau_e \quad (9)$$

From Eq. (8)

$$\xi = -(\tau_i E/RT)([\partial T/T]/[\partial r/r_o])a/r_o \quad (10)$$

Introducing τ_e, gives

$$\xi\varepsilon = -\bar{E}(\partial \ln T/\partial \bar{r}), \text{ where} \quad (11)$$

$\bar{E} = \frac{\tau_i}{\tau_e}\frac{E}{RT}$ and $\bar{r} = r/r_o$.

If T_o is peak temperature at the centre of the hot spot, $\partial \ln T/\partial \bar{r}$ can be approximated by $\ln(T/T_o)$. The associated error for an assumed constant linear gradient, $\partial T/\partial r$, ranges from 0.05% for $\partial T/\partial r$ = -1 K/mm, to 4.7% for -100 K/mm..

The structure of hot spots is largely unknown, but DNS results suggest that the spherical hot spots assumed here are a significant simplification of what is in reality a very complex structure. Essentially r_o can be regarded as the length over which the temperature gradient is almost constant.

The necessity for assumptions surrounding the geometry and structure of hot spots, as well as the need for excitation times that cannot currently be fully validated through measurement, means that a greater uncertainty is attached to values of ε than to those of ξ. However the assumptions can be refined through observation and maintaining a constant value through a range of fuels allows for comparative evaluation and characterisation of fuels or engines independent of variations in turbulent structures in the fluid charge that exist in reality.

In a different context, Lee (2003), Radulsecu (2002, 2007), Sharpe (2003), Shepherd (2009) and co-workers have demonstrated the importance of $\bar{E}$ in assessing the stability of detonations. Low values of both E/RT and τ_i/τ_e are conducive to a spatially more uniform reaction zone, more strongly coupled with the shock wave. These terms are related to ξ and ε in Eq. (11), through the driving hot spot temperature gradient, Shepherd (2009) and Bradley (2012). Higher values of E/R make oblique detonations more unstable, creating an irregular cellular structure, (Radulescu, 2013).

Within the important narrow toe of the peninsula, developing detonations are confined to the lower values of ξ approaching unity. The lower values of ξ_u and the narrowing of the toe at the small values of ε arise because insufficient of the heat release is transferred into the developing acoustic wave. Thermal explosions, at values of ξ below ξ_l, are more rapid, with less severe pressure fronts than those in Fig. 4.3, and temperature gradients that are smaller as demonstrated by Bradley (2002), and Gu (2003).

4.3 Implementations of the $\xi - \varepsilon$ diagram

DNS studies performed by Gu et al. (2003) have found that the diagram created by the dimensionless groups ξ and ε forms a peninsula-like region within which detonation can develop at hot spots. Fig. 4.3 shows the diagram with the peninsula confined by ξ_u and ξ_l. These boundaries were obtained from lengthy DNS of stoichiometric equimolar H_2/CO, chosen for its relatively well understood kinetics. The location of the boundaries could not be directly calculated, but instead involved iteratively mapping the edges of detonative conditions. The hot spot conditions at the very limits of the detonative region are then plotted on the ξ ε diagram and the upper and lower boundaries, ξ_u and ξ_l respectively, drawn through them. The study used a necessarily limited condition range of just a single pressure, 5 MPa, and two temperatures, 1000K and 1100K, imposed by the lengthy process of obtaining ξ_u and ξ_l.

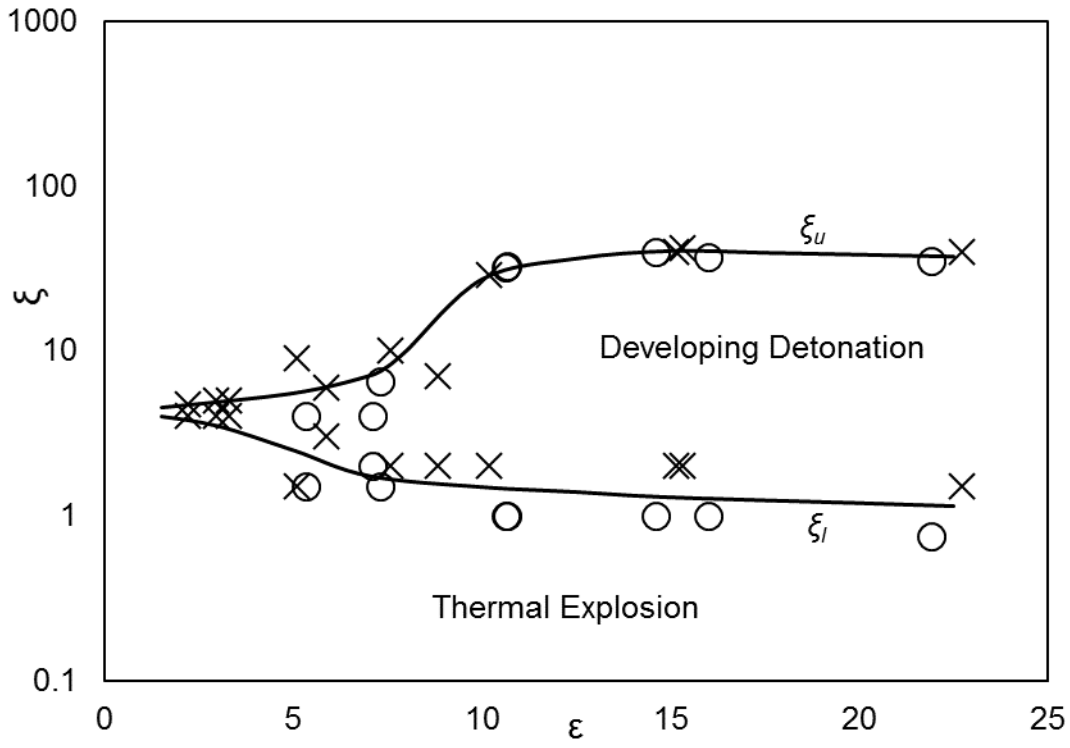

Figure 4.3: ξ against ε diagram showing the region within which Gu's DNS (Bradley et al. 2002) suggests detonation can develop for stoichiometric equimolar H2/CO mixtures at 1000K (×) and 1100K(○).

The peninsula shows a narrow toe at low values of ε, where less reinforcement is available to the pressure wave, making detonation significantly less likely, a very narrow range of ξ values maintain the possibility of detonation.

Further to the initial work of Bradley et al., (2002) and Gu et al. (2003), other groups have implemented the ξ/ε diagram. Kalghatgi (2009) demonstrated that the diagram could be applied to engine performance with increasingly violent knock pushing engine data points deeper into the peninsula created for H_2/CO mixtures, with detonation and super knock occurring inside the peninsula, and severity of detonation increasing toward the lower bound for detonation. Because the peninsula has been constructed on the basis of stoichiometric H_2/CO air kinetics, there was some doubt in its applicability to other fuels. Agreement with these subsequent studies showed that the positions of the peninsula boundaries are unlikely to be drastically different. A

similar study was undertaken by Rudloff et al. (2014) who applied both modelling and experimental results to suggest a shift of the ξ_u and ξ_l boundaries in the positive ε direction. A similar approach is taken by Tanoue et al., (2015) where experimental results from an RCM are combined with modelling in order to provide the necessary data for use with the detonation peninsula, such as excitation time, τ_e. Rather than Rudloff's shift in the peninsula, though, Tanoue et al. (2015) showed general agreement with the existing peninsula, with change in ignition intensity corresponding closely to the original boundaries of the peninsula.

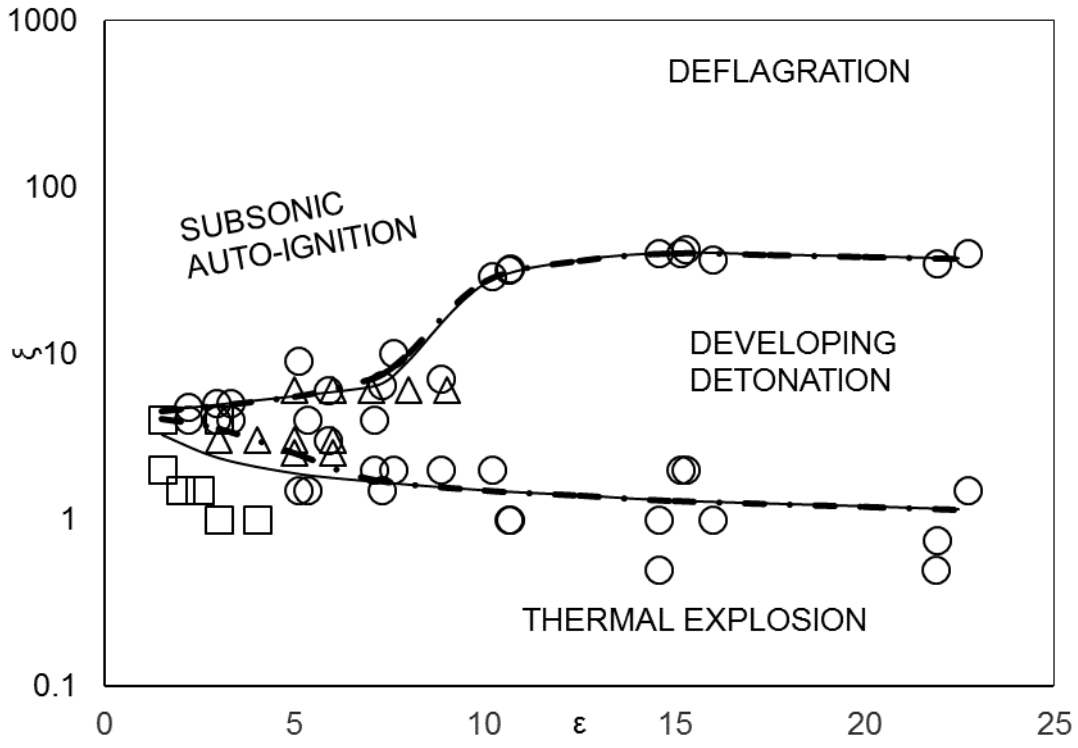

Figure 4.4: ξ/ε regime diagram, for hot spot auto-ignition, showing the detonation peninsulas and other regimes. Symbols indicate data from different fuels ◯: H2/CO/air (Gu et al 2003), □: n-C7H16 /air (Peters et al. 2015), Δ: i-C8H18/air (Peters et al 2015).

The ξ/ε diagram and resulting detonation peninsula have also been investigated by Peters et al., (2014) who applied modelling of n-heptane and i-octane to determine their boundaries iteratively, in a similar way to the original formation of the H_2/CO

peninsula by Gu et al. (2003). Peters found that the peninsulas formed by each fuel were quite similar, needing only small changes to become applicable. Fig. 4.4 shows the peninsula boundaries formed by the H_2/CO data of Gu et al. (2003) with dashed curves, and also those of *n*-C_7H_{16} /air, and *i*-C_8H_{18}/air from the data of Peters et al. (2015) shown as a solid curves. Adjustments were made to the toe of the peninsula, which is a region of high sensitivity due to the relatively small amount of heat release during the residence time of the pressure wave in the hot spot, indicated by small values of ε.

A recent combined LES and experimental study of knock and super-knock in spark ignition engines with *i*-octane made use of the ξ/ε diagram to show the effect of advancing spark timing Robert et al. (2015). As the spark timing was advanced, the cycles become increasingly prone to more and more severe knock and eventually super-knock. When the LES results are plotted on the diagram, shown in Fig 4.5, they show a good agreement with the intensity of ignition recorded in experiments. With a spark timing of 8 CAD after TDC (a) auto-ignitive propagation is recorded with only traces of knock. This can be seen in Fig 4.5 as the results appearing in a vertical band close to the ξ axis. This is a region associated with auto-ignitive propagation, as will be discussed in the following section. When spark ignition occurs at TDC (b) knock becomes more apparent, on Fig. 4.5 this is shown as results with smaller values of ξ, which are associated with increasing intensity until conditions for a thermal explosion are met. There are also some points falling within the detonation peninsula, showing that detonations may be beginning to develop. As spark timing is advanced further, strong knock and super knock are recorded with increasing frequency (c and d), this corresponds to the increasing number of data points within the detonation peninsula

in (c), and in (d) these points are often recorded close to the lower bound ξ_l, where the risk of super knock is greatest.

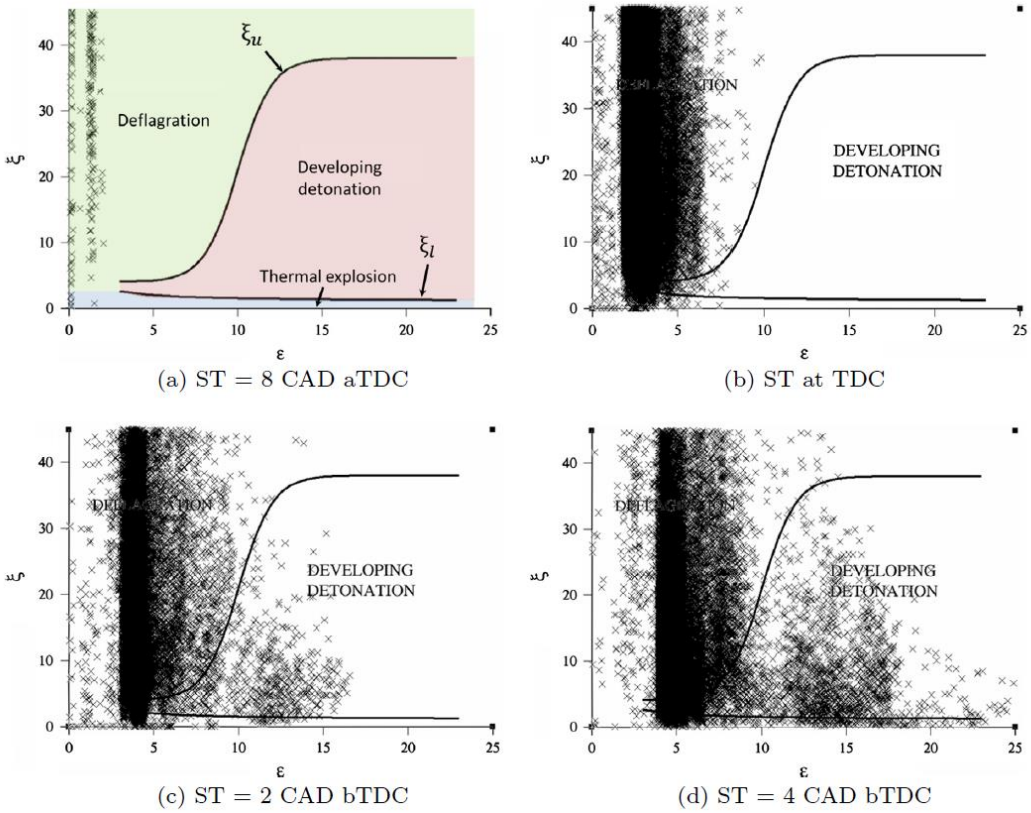

Figure 4.5: The effect of advancing spark timing on ignition intensity, (Robert et al. 2015)

The authors also note that there is uncertainty associated with ε because of the assumed constant length scale of the hot spot, l, in their case, or r_o in the context of this thesis. However, they also note that quite significant changes in length scale, such as $l/2$, did not greatly affect the results relative to the peninsula, with the majority of points still falling within the same regime. The importance of the amplitude of ξ, rather than ε, was highlighted (Robert et al. 2015).

The general applicability of the detonation peninsula is disputed by P. Dai et al (2016) whose data contrasts with that of Peters (2014). The peninsula bounds created by P. Dai et al. suggest an increasing propensity for detonation for *n*-heptane with

decreasing temperature. This may be at least in part to the wide variations in hot spot distance, equivalent to r_o, used in their study.

4.4 The limitations of the temperature gradient simplification

Here the term hotspot has been used to describe a centre of increased reactivity caused by a temperature gradient. This results in the term $\partial T/\partial \tau_i$ in the denominator of equation (8). This causes a numerical problem for fuels that have an NTC in their ignition delay curve, the denominator can become zero. Rudloff (2009) avoids this issue by applying the Arrhenius equation, Eqn. (1), to the fuel's ignition delay, effectively removing the NTC region from the curve. This removes the possibility inflection points in the curve where $\partial T/\partial \tau_i$ would instantaneously be zero. While this solves the numerical problem, it also reduces the effectiveness of the peninsula with real fuels that have such an NTC region or nonlinear behaviour. A more robust approach is to remove the simplification and instead consider the hotspot as an ignition delay gradient, $\partial \tau_i/\partial r$, directly.

If a simplified hotspot is considered whose temperature range covers a point of local minimum or maximum in τ_i, such as in an NTC region, then $\partial T/\partial \tau_i$ at that point is zero, causing Rudloff's numerical problem. However, by considering instead $\partial \tau/\partial T$, we can see that the hot spot is in fact not a simple hot spot. A maximum in τ_i produces two converging reaction fronts within the radius of the hot spot, while a minimum produces an initial ignition surface geometry at a radius from the centre of the simplified temperature gradient hot spot before propagating both towards the centre point and out from the ignition surface geometry.

For the same fuel, hot spot temperature gradients which fall outside the NTC region, or over relatively constant $\partial^2\tau_i/\partial T^2$, the temperature gradient may still be used successfully to represent a hot spot.

This limitation is also applicable to an ignition delay gradient created through other means, such as equivalence ratio or pressure gradient, or by a complex combination of factors, as in reality.

4.5 The deflagration boundary

As ξ increases above the upper limit of the detonation peninsula, ξ_u, the propagation of reaction after hot spot auto-ignition tends more toward deflagrative burning. Auto-ignitive propagation is not precluded outside the peninsula, but the accompanying pressure pulses will be relatively weak with no transition to detonation.

Sankaran et al. (2005) explored a transitional region between deflagrative and auto-ignitive propagation regimes after hot spot auto-ignition with DNS in turbulent homogeneous mixtures. The simulations showed a dependence on the temperature gradient, $\partial T/\partial r$, whereby a small temperature gradient creates an auto-ignitive velocity that is large relative to the laminar flame speed of the mixture. Increasing the gradient reduces the rate of propagation by auto-ignition until it is overtaken by that of deflagration controlled by molecular transport processes. Sankaran et al. (2005) report that deflagrative flames initially accounted for only 17% of heat release rate with auto-ignitive propagation forming the remainder. This suggests that both propagation modes attained critical radii but that the auto-ignitive mode was dominant. Larger, less stretched kernels were observed to develop, while smaller, more stretched kernels were unable to survive.

Sankaran et al. (2005) defined a transition parameter, β, as the deflagration velocity, u_d, normalized by u_a. As β is increased, deflagration becomes more dominant. It must also be noted that initial values of u_d are undeveloped and so lower the rate of a developed deflagrative propagation.

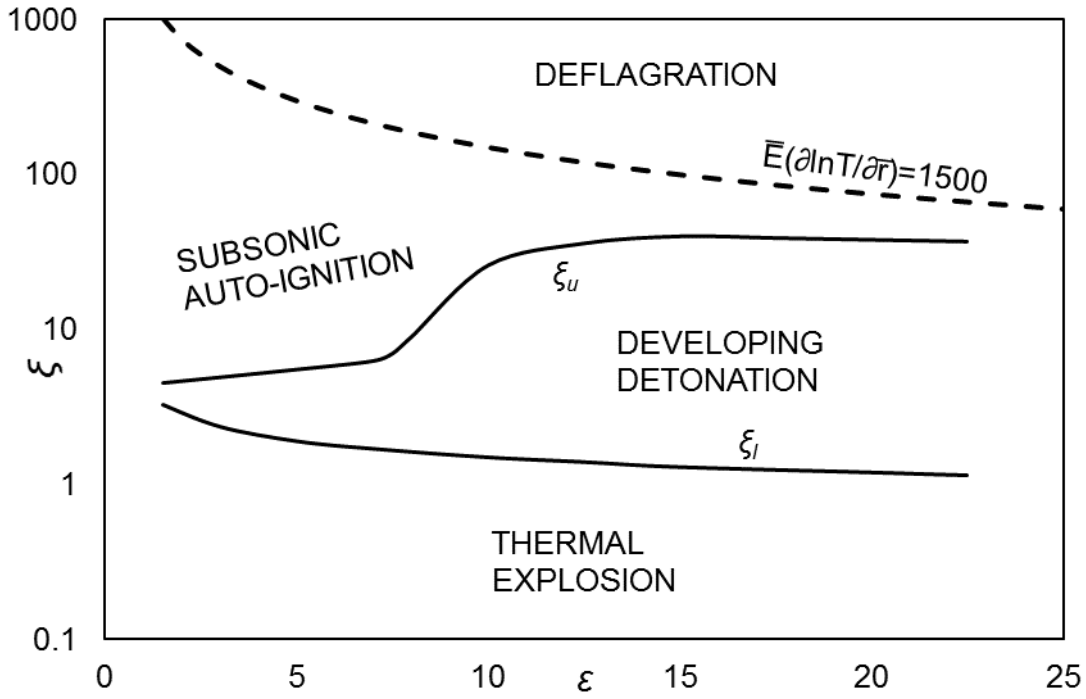

Figure 4.6: Detonation peninsula with the addition of auto-ignitive to deflagrative propagation boundary

Following earlier studies by Walton et al. (2007) and Mansfield and Wooldridge (2014) of *i*-octane auto-ignition found that, with a 0.59 H_2/0.41 CO/N_2/air syngas mixture, at ϕ = 0.5, β became greater than unity at $\partial T/\partial r$ ~ -5 K/mm. Assuming a hot spot radius, r_o, of 3 mm and $\bar{E}$ = 110. 10^3 at 1100K, this temperature gives $\bar{E}(\partial \ln T/\partial \bar{r})$ = 1490. A generalized relationship for this parameter = 1500 is shown on Fig. 4.6, as a tentative and approximate threshold for the onset of deflagration. This threshold should be interpreted as a transitional region, rather than a sharp boundary

curve, as a broad regime exists within which both modes of propagation can coexist, as demonstrated by the DNS of Sankaran (2005) and Minamoto (2014), but it is represented by a curve here for simplicity and due to the uncertainties involved.

Shown on Fig. 4.7 are further curves of constant $\xi\varepsilon = -\bar{E}(\partial \ln T/\partial \bar{r})$, from eq. 11, which are valuable indicators for intensity of ignition, consisting of the detonation stability parameter $\bar{E}$ and the temperature gradient $(\partial \ln T/\partial \bar{r})$. As $\bar{E}$ becomes small the stability of detonation increases, while small temperature gradients increase likelihood of detonation and super knock.

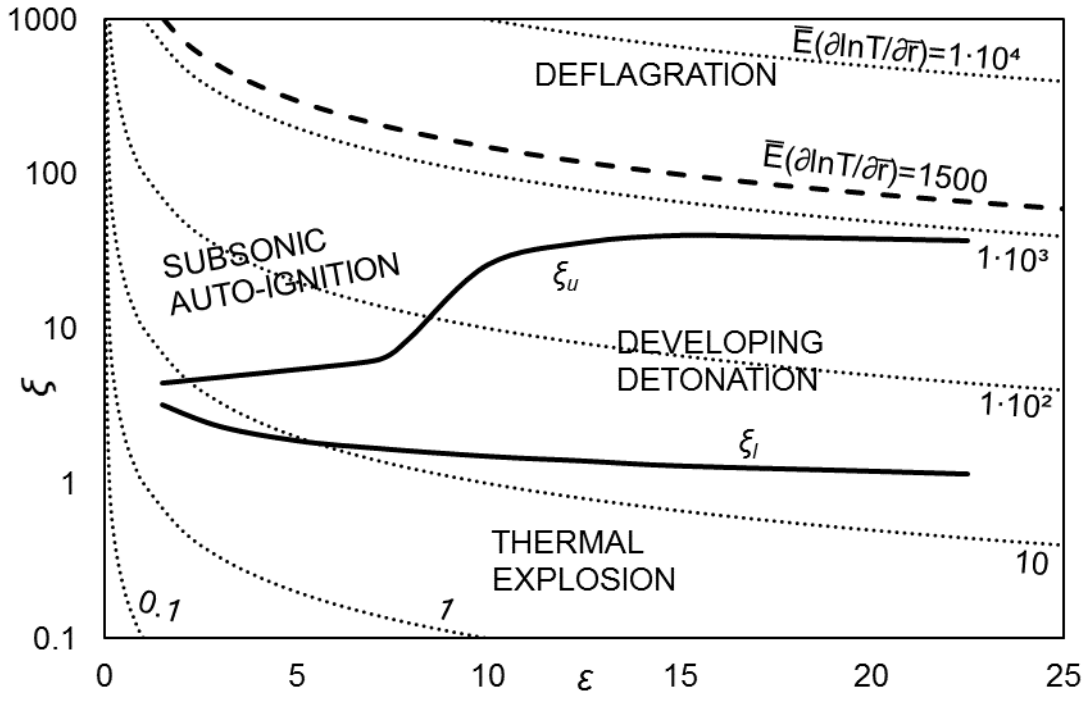

Figure 4.7: The ξ/ε diagram with addition of curves of constant values of $\bar{E}(\partial lnT/\partial \bar{r})$

The dominance of the auto-ignitive mode, $\beta < 1$, involved additional criteria and these can arise in two contrasting ways, which are independent of u_a, the first is when u_d, is either a laminar or turbulent burning velocity, significantly less than u_a. The second

occurs when, with increasing turbulence, u_d, and β, after attaining a peak value with $\beta > 1$, then decline, due to the onset of localised flame extinctions arising from the increasing flame stretch rate, with $\beta = 0$ at complete flame quench. This regime is identified by Abdel-Gayed et al. (1989) and Bradley et al. (2007). It has been shown to be suitable for controlled auto-ignitive engine combustion by Bradley (2008).

4.6 Conclusions

The peninsula diagram originally developed by Bradley has been shown to be more general than originally proposed. The diagram is at least also applicable to the primary reference fuels *i*-octane and *n*-heptane with minimal changes to the peninsula boundaries.

A third dimensionless group, $\bar{E}$ has been formed which encapsulates the major properties of the fuel. Small values of $\bar{E}$ are conducive to detonation stability, and when combined with small temperature gradients are indicative of high ignition intensity.

In addition to the boundaries ξ_u and ξ_l, which enclose the region within which detonations may develop, a further boundary has been established between auto-ignitive and deflagrative propagation modes.

The dimensionless parameter ε, while bearing the most uncertainty is also the most resistant to variation. A change by a factor of two in ε for practical applications will often not cause significant changes to a point's location relative to the peninsula. Exceptions may be found if a point lies close to the narrow toe of the peninsula.

5 The ξ/ε Diagram for Fuels and Engines

5.1 Introduction

The previous chapter covered the development and general presentation of the detonation peninsula on the ξ/ε diagram. The need to characterise both fuels and engines was also discussed in the introduction to this thesis. This chapter will cover the application to both fuels and engines of the ξ/ε diagram and its usefulness in this characterisation. The diagram is applied to a variety of different fuels, including paraffins, aromatics and surrogate gasoline and a variety of disparate engines including controlled auto-ignition, CAI, spark ignition and turbo charged spark ignition engines. In addition, an RCM is included.

5.2 The relationship of ξ to T for different fuels.

Shown in Fig. 5.1 are the profiles of the ξ values of several fuels over a range of temperatures and at a constant pressure, P, of 4 MPa and equivalence ratio ϕ=1. The values are evaluated for a constant temperature gradient of -2K/mm using τ_i from data sources: OI 105 (Kalghatgi, 2009), PRFs (Bradley & Head, 2006), (Peters et al. 2013), ethanol (Lee et al. 2011), toluene (Davidson et al. 2015), methane (Lutz et al. 1988), and hydrogen (Browne et al. 2005). Values of ξ indicative of severe detonations or super-knock are generated when the auto-ignition velocity, u_a, is sufficiently close to the acoustic velocity, a, at which the pressure pulse generated by the reaction propagates, giving values close to unity.

In Fig. 5.1 no fuel reaches unity for temperatures lower than 1000K, with fuels such as H_2 and CH_4 remaining in excess of ξ = 5 beyond 1100K. Other fuels that show good resistance to severe detonation include toluene, H2/CO, and ethanol.

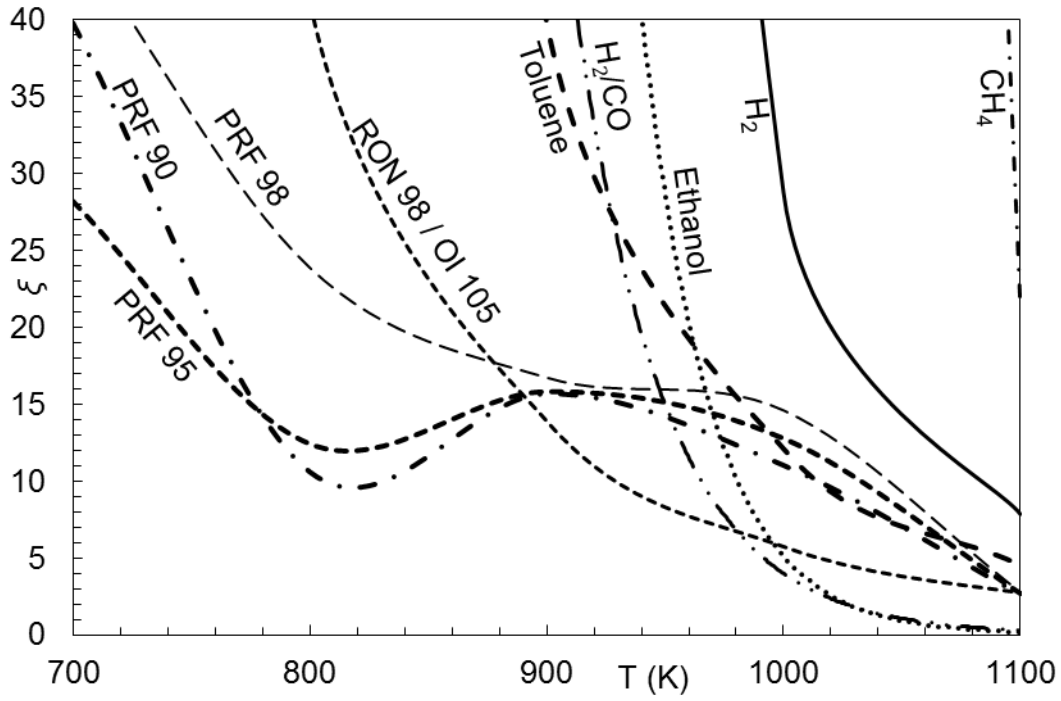

Figure 5.1: Calculated values of ξ at 4 MPa and = -2 K/mm for stoichiometric mixtures of air with various fuels.

Despite the similarity in RON, the PRF 98 and OI 105 fuels show considerable differences. OI 105 shows much less propensity to detonate until temperatures in excess of 900K are reached. Beyond this point a region of negative temperature coefficient, NTC, makes PRF 95 slightly less prone to detonation.

Less severe detonations, which may even remain benign, can continue to develop for values of ξ greater than unity given the correct temperature gradient and hot spot radius. The PRF 90 and 95 fuels could potentially develop to detonation through the entirety of the temperature range given in Fig. 5.1 if the hot spot radius is sufficient.

The ability to map the dimensionless group values over a range of conditions is a distinct advantage over the octane rating systems, RON and MON, and other similar systems, which are constrained to narrow bands of conditions by their nature.

5.3 The ξ/ε diagram for fuels

In the previous chapter it was shown that when $\bar{E}(\partial \ln T \partial/\bar{r})$ exceeds 1500, at the higher values of ξ, deflagration becomes significantly more probable than auto-ignition. This relationship and that for a lower value of $\bar{E}(\partial \ln T \partial/\bar{r})$ = 50, extensively within the peninsula, are shown in Fig. 5.2. The lower values of $\bar{E}(\partial \ln T \partial/\bar{r})$ are associated with smaller temperature gradients, and therefore higher propensity to detonate.

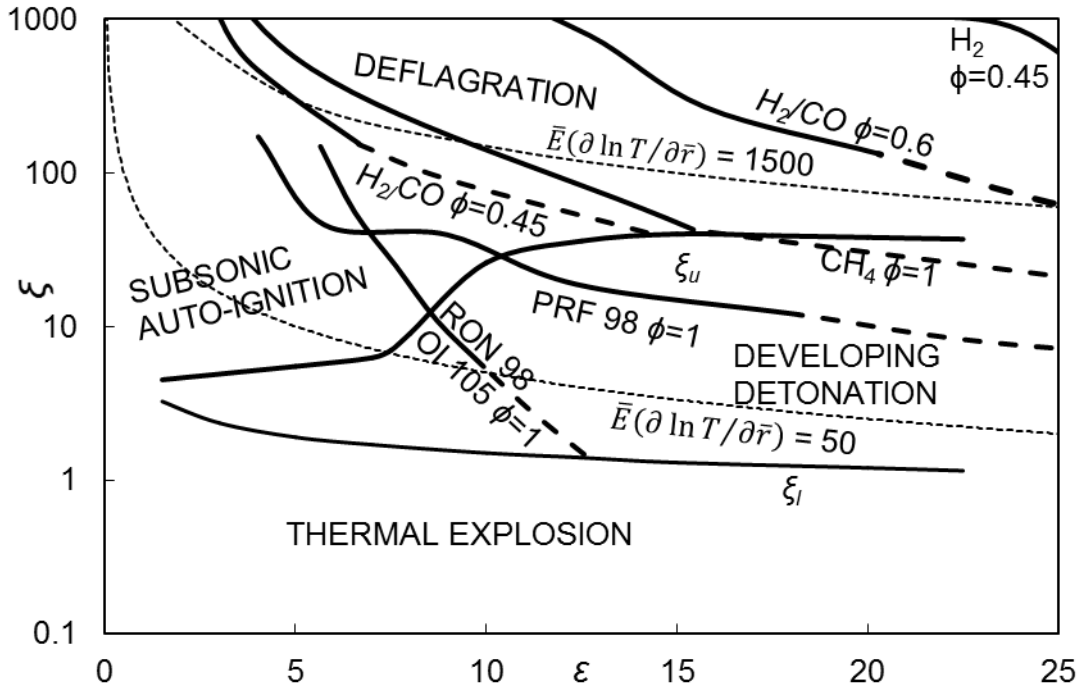

Figure 5.2: Isentropic compression curves for different fuels showing propensity for detonation.

The primary purpose of Fig. 5.2 is to assess the propensity of different fuel/air mixtures to develop a detonation after hot spot auto-ignition, during isentropic compression from 800K and 1.0 to 10 MPa and, ultimately, 1100K at 15 MPa. Dashed curves cover the later stage of compression between 10 and 15 MPa, associated with combustion regimes in turbo-charged engines. Data sources of τ_i and τ_e for the different *P* and *T*, are given in Table 5.1.

Sometimes the limited data on τ_e required extrapolations of existing data. This was especially so in the case of CH_4, with its restricted pressure range, for which the data of Lutz et al. (1988) were among the first τ_e data to be calculated. The low temperature and pressure conditions of the available data made it necessary to compute new detailed chemical kinetic values for CH_4 excitation times, the computations for which were carried out by Gorbatenko (2016).

Mixtures studied include H_2/air, at an equivalence ratio, ϕ, = 0.45, equi-moles of H_2 and CO with air at ϕ = 0.5 and 0.6, which may has potential applications outside of the more general automotive theme of this section, in reducing iron ore to iron, together with a PRF of 98, at ϕ = 1.0.

Fuel	ϕ	τ_i	τ_e
H_2/CO	0.5, 0.6	(Gu et al., 2003)	(Gu et al., 2003)
H_2	0.45	(Browne et al. 2005)	(Browne et al. 2005)
PRF 100, 98	1	(Bradley & Head 2006), (Peters et al. 2013)	(Peters et al. 2013)
CH_4	1	(Lutz et al. 1988), (Gorbatenko 2016)	(Lutz et al. 1988), (Gorbatenko 2016)
OI 105	1	(Kalghatgi et al. 2009)	(Kalghatgi et al. 2009)

Table 5.1: Sources of data for τ_i and τ_e between 3 and 15 MPa, 800 and 1100K.

The DNS studies of Sankaran et al. (2005) and Yoo et al. (2011) show that the reality of a hot spot is far more complex than the simple spherical idealization and linear temperature gradient defined here. Complex turbulent interactions together with the potential for auto ignition gradients to form based on a number of variations in the charge mixture either individually or in combination with each other could lead to complex hot-spot geometries and ignition delay profiles. In addition, the scope of this study is restricted to a single hot spot in isolation. In reality, it is more likely that multiple hot spots are active in a similar time frame and potentially interacting with each other. Detonation might not develop solely at one hot spot, but its pressure pulse might reinforce a secondary or even tertiary hot spot, indications of this are observed by Dingle et al. (2014).

In the present context, those sizes and shape that auto-ignite within the detonation peninsula are most relevant. In engine geometric considerations are suggested as r_o = 5 mm, and dT/dr = -2 K/mm. The value of E for heavy knock was estimated to be 7,000. With dT/dr = -2 K/mm, this gives a value of $\bar{E}(\partial \ln Y/\partial \bar{r})$ = 17.5, which is consistent with its location within the toe of the peninsula in Fig. 5.3. Together with the consistency of the available engine and fuel test results for a variety of engines and fuels, this confirmed the suitability of these hot spot values, for bench marking engine knock in Figs. 3 and 4. In another context, for example when investigating hazards presented by the storage or transport of a fuel, a much larger hotspot with a relatively small temperature gradient might be required.

All fuels were mixed with air. H_2 and H_2/CO mixtures show the most resistance to detonation, with none of conditions, even at the higher pressures, entering the

detonation peninsula. Similarly, CH_4 largely avoids the peninsula, only crossing into the region of developing detonation under severe conditions with high values of ε and at high temperature and pressure. The absence of alcohol fuels, such as ethanol, a popular component in modern gasolines, and *n*-butanol, a possible future fuel component, is due to the dearth of excitation time data.

The 98 PRF, ϕ = 1, entered the detonation peninsula at a pressure of 6 MPa and 925K, whereas the surrogate gasoline, OI = 105, ϕ = 1, RON = 98, was able to attain a pressure exceeding 7.5 MPa and a temperature of 950K prior to such entry. Not only does the latter mixture have a superior anti-knock performance, but it is an interesting example of a negative value of Kalghatgi's (2009) *K* in Eq. (2), chapter 1, with an OI value that is higher than the RON rating of the fuel.

Characterisation for fuels is relatively straightforward. All that needs to be determined is a standardised range of conditions such as ranges of *T*, *P*, and temperature gradient. The fuel can then be mapped over these ranges for given hot spot radii. The main barrier to this method is the need for excitation time data.

5.4 The ξ/ε diagram for engines

As well as fuels, the ξ/ε diagram can also be applied to the characterisation of engines. Here the amount of data available is again limited, and all available data with sufficient detail is condensed into Fig. 5.3, which shows data on engine knock and near-knock, drawn from a variety of studies. Table 2 gives the symbols for type of engine, sources of data, the fuels, auto-ignitive modes, maximum pressures and temperatures. Some data are new such as that of Rudloff et al. (2013) and Tanoue (2015), some have been

employed in earlier studies by Bradley and Head (2006), Bradley (2012), Wang et al (2014, 2015), Rothenburger (2012) and Manz (2012).

	Type	Fuel	Auto-ignitive Mode	*P* MPa (max)	*T* K (max)	Ref.
+	Single cylinder – Roots blower	PRF 84 ϕ = 0.25	Controlled auto-ignition	6.52	729	(Bradley & Head, 2006) (Bradley 2012)
◊	Single cylinder – NA	RON 97	Deflagration - super knock	2.74	1000 (estim.)	(Rudloff et al. 2013)
Δ	RCM	C_4H_{10} with DME additive	Deflagration - super knock	5.55	835	(Tanoue et al. 2015)
○	S.I. engine - turbo	RON 95 / OI. 105	Deflagration - super knock	12.8	1057	(Rothenberger, 2012)
□	S.I. engine - turbo	RON 94	Light knock - super knock	10.91	949	(Wang et al, 2014) (Wang et al. 2015)
×	S.I. engine - turbo	RON 98 / OI. 107	Super knock	13.3	926	Manz (2012)

Table 5.2: Table 5.2: Engine and apparatus presented in Fig 5.4 including fuel, maximum *T* and *P* and mode of reaction.

Engine types shown on Fig. 5.4 include controlled auto-ignition, conventional spark ignition, turbo charged, and a rapid compression machine, RCM. Operational points at the highest cylinder pressures are shown in the figure. A + indicates controlled auto-ignition, otherwise ignition intensity increases with the level of fill of the symbol, an unfilled symbol shows no knock, a half-filled symbol moderate knock, and a filled symbol "super-knock" induced by pre-ignition. In general, an increase in pressure increased the severity of knock. All operations with controlled auto-ignition were at equivalence ratio ϕ = 0.25, with PRF 84 fuel, and exhaust gas recirculation, to attain a sufficient temperature for auto-ignition. Otherwise ϕ = 1.0.

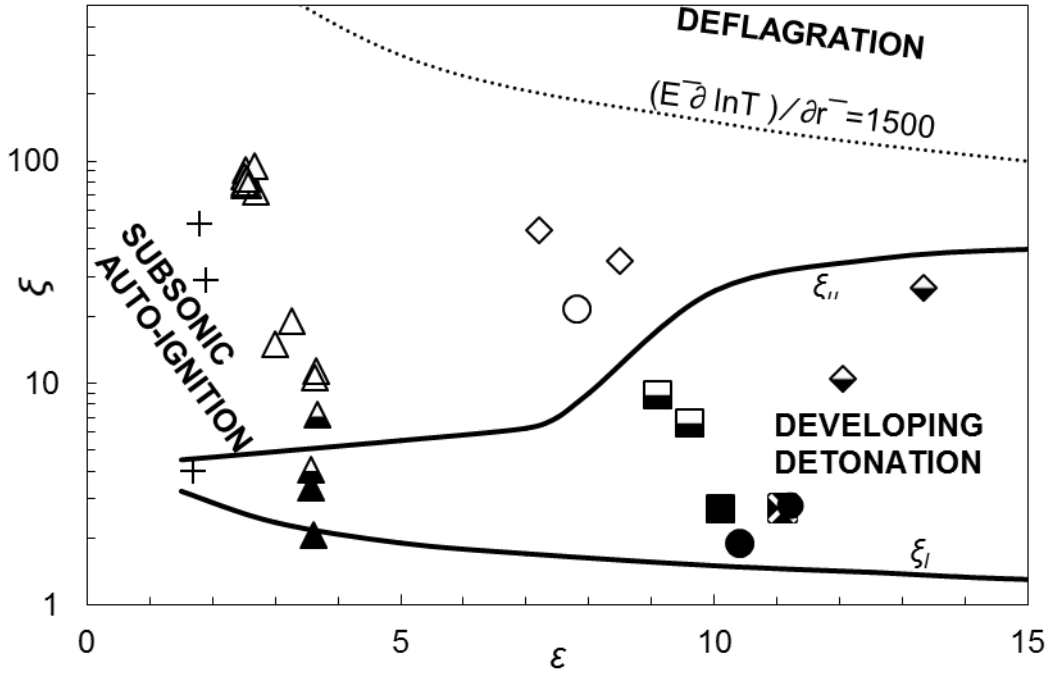

Figure 5.3: Engine operational points close to maxima *P* and *T* for different engines and fuels, as listed in Table 5.2.

Data points indicated by Δ are from a rapid compression machine study by Tanoue et al. (2015), in which maximum knock pressure amplitudes varied as $\xi^{-1.923}$, close to the

estimate of ξ^{-2} by Bradley et al. (2009). The diverse operational conditions show that entry into the detonation peninsula is associated with the onset of knock, which can become severe.

Conditions that are conducive to benign auto-ignitive burning are low burning velocities and temperatures just high enough for auto-ignition, such as lean combustion and with exhaust gas recirculation. The regime has been identified as one of controlled auto-ignition, flameless combustion, and MILD combustion (moderate intense low-oxygen dilution). CAI engine points, +, on Fig. 3 are in this regime.

Interestingly one of the CAI points appears within the very end of the currently open toe of the peninsula yet does not show any sign of developing to a detonation. Dai et al. (2016) suggest that the peninsula is not general, but dependant on factors such as heat release and is affected by ϕ. This contrasts with findings here, especially given the increased propensity for detonation with decreasing temperature that Dai et al. imply for *n*-heptane. The open end of the toe is currently only loosely defined; further investigation of this small region may result in a closed peninsula, or in a region where multiple modes of propagation may coexist, as is the case for the region of transition between auto-ignitive and deflagrative propagation modes.

The spark-ignited engines, all with similar fuels, RON 94-98, behave quite similarly with the exception of the non-turbo charged spark ignited engine. The maximum value of *P* experienced by the non-turbo charged engine more than 8 MPa less than that with turbo charging. Even when the non- turbo charged engine crosses into the peninsula it maintains a relatively high value of ξ, far from the region in which super knock might be expected. In contrast those engines with turbo charging cross into the peninsula quite quickly, moving through light knock to potentially damaging detonation and super knock at values of ε of about 10.

To turn a diagram such as Fig. 5.4 into a characterisation would require some form of standardisation, which at the present time can only be a limitation for any worthwhile characterisation technique. Current real gasolines are both complex and varied by nature, meaning that any surrogate or approximation must vary with the fuel currently available to remain relevant. Until practical engine fuels are more uniform in composition this is a limitation any method for engines must face. The complexity of gasolines poses another problem for the ξ/ε diagram, presently the only reliable way to obtain τ_e data is by detailed modelling, for which gasoline is overly complex with large molecules and diverse constituents. An estimated τ_e might be appropriate, since the ξ/ε diagram has been shown to be less sensitive to variations in ε. The method retains advantages in that a wide range of conditions can be explored, and profiles for the test fuel could be overlaid on experimental points to extrapolate to further operating regimes.

5.5 Conclusions

The ξ/ε diagram has been applied to both fuels and engines. The operational regimes observed experimentally agree with the respective location of data on the ξ/ε diagram. This confirms further the global nature of the diagram and the assumptions made connected to hotspot geometry and temperature gradient.

Characterisation can be carried out with the ξ/ε diagram for fuels and engines, however while the characterisation of fuels is relatively simple, obtaining sufficient τ_e data for such a characterisation is not trivial. Characterisation of engines is less simple due to wide variations in real fuels.

Of note is the resistance of methane to entry into the detonation peninsula. This resistance is an inherent property of methane, but it also has an additional advantage in that, as a gaseous fuel it does not exhibit the problems associated with the stripping of lubricant oil from piston rings.

There are still some areas that are not well defined. In particular the important narrow toe of the peninsula is currently open ended, with no clear indication of where the boundary might lie perpendicular to the ε axis, if there is indeed a boundary.

6 Turbulent burning regimes and the ξ/ε diagram

6.1 Introduction

The previous chapters discuss the application of the ξ/ε diagram for determining the mode of reaction propagation from an auto-ignitive hotspot. This approach is applicable to a broad range of conditions but is restricted to laminar burning conditions. Turbulent burning increases complexity as the turbulence changes the behaviour of the flame. As the turbulence acts on the flame front it causes wrinkling of the flame which has the effect of accelerating the flame front. If turbulence is then increased incrementally, the acceleration will also be increased up to a point at which the strain rate in the flame front inhibits the flame and eventually causes quenching.

The turbulence itself is quantified by the parameter *u'*, which is the mean turbulent velocity, and by the integral turbulent length scale *l*. Instead of the laminar burning velocity, u_l, the turbulent burning velocity, u_t, is taken. The convective transport rate relative to the reaction rate is represented by Karlovitz stretch factor, *K*, such that for values of $K << 1$ the chemical reaction rate is dominant and combustion is laminar.

In order to determine important regimes such as quench, the approach must be extended to include turbulent conditions. The existing diagram of Mansour et al. (2013) serves as the foundation for the turbulent regimes and the unification of this with the existing diagram for laminar conditions. This diagram was constructed from the results of an extensive experimental study conducted on the Leeds MKII Fan Stirred Internal Combustion Bomb. And succeeds the less informative Lewis number diagram traditionally used at Leeds (Bradley et al. 2011). The diagram expresses $U=u_t/u'$, as a function of strain rate Markstein number, Ma_{sr}, and Karlovitz stretch

factor, *K*. The combination of both ξε and UKdiagrams will provide coverage of both laminar and turbulent burning regimes.

6.2 The Complimentary *U* – *K* diagram

The characterization of fuels and engines is thus far incomplete and requires further data for properties such as burning velocity and strain rate Markstein number, Ma_{sr}. These properties are included in a complimentary *U*/*K* diagram by Mansour (2013), which gives a more complete overview of fuel or engine behaviour when paired with the ξ/ε diagram.

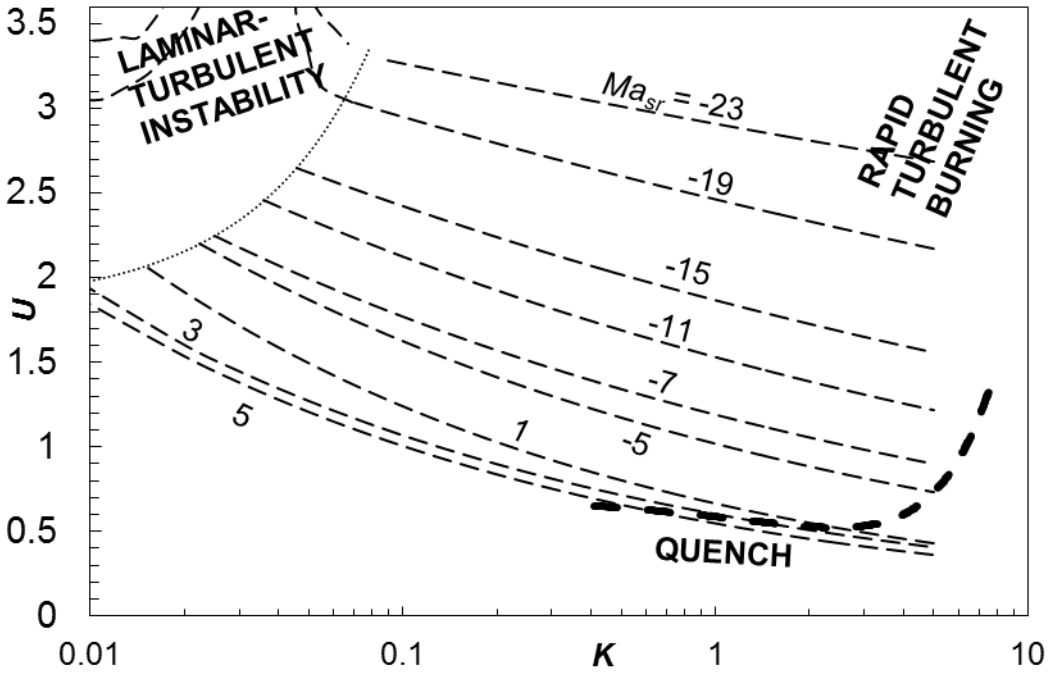

Figure 6.1: The *U*/*K* diagram for turbulent burning, Mansour et al. (2013).

Here *K*, unlike that of Eq. (1), is the Karlovitz stretch factor, while *U* is the turbulent burning velocity, u_t, normalized by the rms. turbulent velocity, *u'*. The *U*/*K* diagram, as well as Ma_{sr} and burning velocities, can be indicative of turbulent combustion

regimes such as those of flame quench and instability. Overlapping links between the ξ/ε and U/K diagrams facilitate identification of the different combustion regimes, and assessment of the knock resistance of different fuels. Both diagrams can include the relative magnitudes of the turbulent burning velocity and the auto-ignitive velocity that can arise at a possible igniting hot spot.

The ratio of the turbulent burning velocity, u_t, to the effective rms turbulent velocity, u', that allows for flame kernel development, U, is expressed as

$$\frac{u_t}{u'} = U = \left(\frac{u_t}{u_l}\right)\left(\frac{u_l}{u'}\right) \quad (1)$$

Where u_l is the laminar burning velocity. The Karlovitz stretch factor, K, as in Mansour (2013) is given by

$K=0.25(u'/ul)^2 R_l^{-1/2}$,

here R_l is the turbulent Reynolds number, $R_l = \frac{u'l}{\nu}$, with l the integral turbulent length scale and ν the kinematic viscosity, giving

$K=0.25(u'/u_l)^2 (u'l/\nu)^{-1/2}$,

and from this;

$$K=0.25(u'/u_l)^{2/3} (u_l l/\nu)^{-1/2} \quad (2)$$

This gives rise to the expression that relates turbulent to laminar burning velocities:

$$u_t/u_l = U\left[4K(u_l l/\nu)^{0.5}\right]^{2/3} \quad (3)$$

With $\xi = a/u_a$, and division by u_a:

$$(u_t/u_a) = U(4K)^{2/3}(ul/\nu)^{1/3}(u_l\xi/a), \quad (4)$$

and as $\xi = u_a/a$,

$$u_t/u_a = \xi(u_l/a)U\left[(K/0.25)(u_l l/\nu)^{1/2}\right]^{2/3} \quad (5)$$

$$(u_t/u_a\xi) = U(4K)^{2/3}(u_l/a)(u_l l/\nu)^{1/3} \quad (6)$$

Let $c = (u_l/a)(u_l l/\nu)^{1/3}$, characterizing in-cylinder properties. (7)

The U/K diagram is now enhanced with curves of constant $u_t/u_a\xi$ and is shown in Fig. 6.2. The ratio of deflagrative to auto-ignitive propagation velocity, u_t/u_a, is an indicator of which of these is dominant in the propagation of reaction initiated at a hot spot. It has been employed in both direct numerical simulations, DNS, by Sankaran et al. (2005) and experiments by Mansfield et al. (2015). It is now possible to use this diagram in conjunction with the ξ/ε diagram to identify further regimes of propagation, including quench, laminar-turbulent instability and rapid turbulent burning.

Values of c were found from estimated values of u_l, a, l and ν within the peninsula, with u_l = 0.4 ms^{-1}, a = 510 ms^{-1}, l = 0.002 m, and $\nu = 1.5.10^{-5}$ m^{2}s^{-1}. These give c = of 0.00636. Contours of both $\left(u_t/u_a\xi\right)$ and Ma_{sr} are plotted on the new synthesised diagram of plots of U against K, in Fig. 6.2, based on this value of c. For a different value of c, say c', the revised value for the contour would be that on Fig. 6.2 multiplied by $c'/0.00636$. Over most of the diagram, mixed combustion is possible, dependent on the value of ξ. Within the flame quench regime, only auto-ignitive burning is possible.

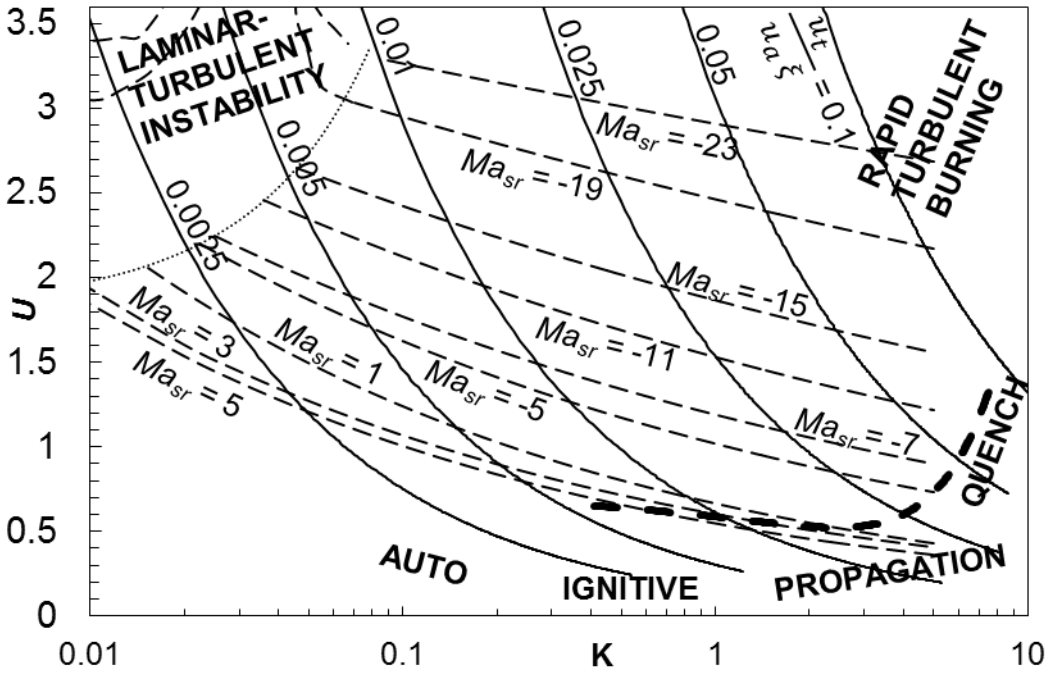

Figure 6.2: The *U*/*K* diagram with curves of constant Ma_{sr}, and ($u_t/u_a\xi$).

The ξ/ε diagram can be used to identify those regimes controlled by auto-ignition and flame propagation. Further regimes controlled by turbulent burning require the additional combined use of the *U/K* diagram. The constant curves of $u_t/u_a\,\xi$ shown on Fig. 6.2 indicate the relative dominance of turbulent burning and auto-ignitive propagation, with higher values likely to indicate a more rapid turbulent burning velocity, u_t, and lower values a higher auto-ignition velocity, u_a.

Over the majority of the diagram, mixed combustion is possible, but within the quenching region, the only possible mode of propagation is auto-ignitive. Auto-ignitive operation of an engine here is beneficial because the location inside the quench regime makes detonation impossible, while auto-ignitive propagation can continue. Combination of the *U*/*K* diagram and the ξ/ε diagram therefore makes it possible to identify regimes suited to operation of specialist engines such as controlled auto ignition, CAI, engines.

CAI engines, also commonly known as “homogeneous charge compression ignition,” HCCI, engines despite the practical impossibility of a true homogeneous charge, commonly operate in the central region of the *U*/*K* diagram in moderately turbulent conditions. In the region indicated on Fig. 6.2 as “auto-ignitive propagation”, quenching of the flame is caused by high turbulence stretching the flame front to the point of extinction. This high stretch, indicated by an increasingly positive strain rate Markstein number, $Ma_{sr,}$ maintains a condition in which a propagating flame cannot survive. This prevents coupling between the reaction and pressure waves, removing the possibility for detonation. Auto-ignitive engines can operate outside this region, maintaining relatively low *U* and *K* values, but run the risk of detonating. Spark ignited internal combustion engines operate at higher values of *U* and *K*, approaching the “rapid turbulent burning” region on Fig. 6.2 with quite large negative Ma_{sr}, indicating minimal stretch in the flame front. Their dependence on a propagating flame front makes this type of engine unsuitable for operation in a region of quenching flames.

6.3 Application to a fuel

An example isentropic compression condition curve of a fuel that is in a regime of turbulent burning is shown dotted and arrowed, showing direction of compression, on Fig. 6.3. The curve is constructed from the assumed turbulent burning velocity of a stoichiometric *i*-octane/air mixture compressed up to the knocking condition at 10 MPa. The compression takes place with assumed u' = 3 m/s and l = 2 mm. Laminar burning velocity and Ma_{sr} data at high *P*, and *T* are rather more scarce than τ_i data and are extrapolated from those of Bradley et al. (1998).

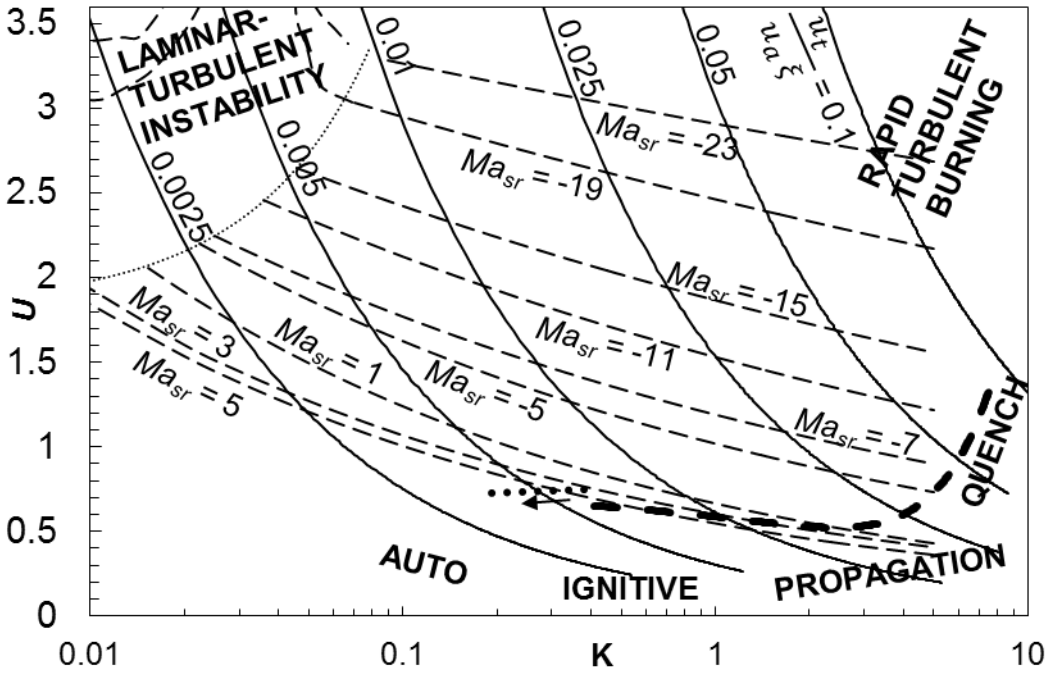

Figure 6.3: Turbulent and auto-ignitive burning regimes on a *U*/*K* diagram, with contours of Ma_{sr} and $(u_t/u_a\xi)$.

The condition curve cuts the $(u_t/u_a\xi)$ contour at a value of 0.005. Consequently, even with ξ = 10, the u_t/u_a ratio would only be 0.05 and auto-ignitive propagation would prevail at any sufficiently active hot spot. Here the dominant influence is that of ξ. In contrast, under atmospheric conditions ξ would be very large and u_t would dominate. A more complete understanding of the deflagrative/auto-ignitive regimes and their burning rates must be supplemented by the ξ/ε diagram, where intensity of ignition can also be assessed.

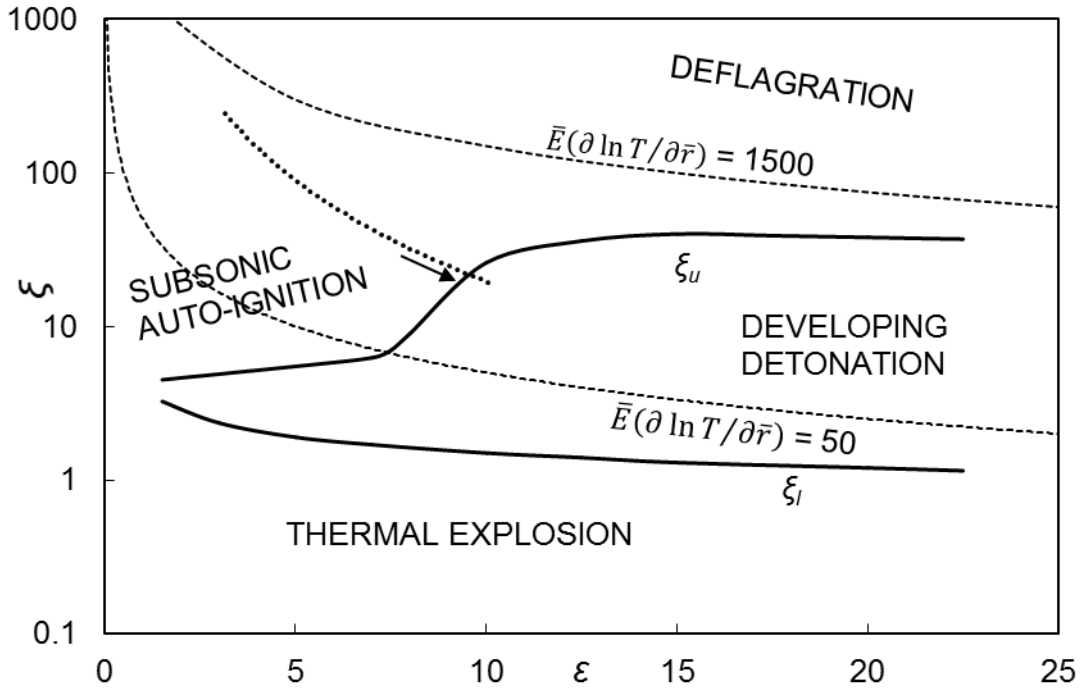

Figure 6.4: ξ/ε diagram showing the same condition curve as that in Fig. 6.4, arrow indicated direction of compression.

The same condition curve shown in Fig.6.3 is also shown on Fig. 6.4, residing predominantly in the auto-ignitive portion of the diagram, but at the end of the compression, the curve enters the detonation peninsula. Whether this is indicative of a detonation is, in this case, not entirely clear due to the proximity of the compressed end of the curve to the quenching regime in Fig. 6.3. Extension of the quench boundary might see the portion of the curve that is within the detonation peninsula on Fig. 6.4 also fall within the quench regime in Fig. 6.3, potentially prohibiting detonation. An increase in *u'* would serve to push the curve further towards the quenching region, into the region of the diagram denoted as being conducive to auto-ignitive propagation. Conversely, a reduction in this value would move the curve away from the quench boundary, making detonation a more probable outcome.

6.4 Conclusions

The combined *U/K* and ξ / ε diagrams indicate the different regimes of combustion. The use of the detonation peninsula gives good indication of the ignition intensity, while the U/K diagram is indicative of regime when combustion is turbulent.

The combination of both the *U/K* and ξ / ε diagrams provides indication of regime beyond the capabilities of empirical systems such as RON and MON and toluene reference fuels, TRF. Use of fundamental fuel properties allows application of the diagrams at any condition and with any fuel.

The combined diagrams are particularly effective in identifying operational regimes for specialized internal combustion engines, such as controlled auto-ignition engines, which can use normally restrictive regimes, such as quench to their advantage.

7 Conclusions summary and future research

7.1 Introduction

The out-dated and inherently limited octane numbering system is still in use despite its well-known shortcomings. Although other systems are in use (such as the AKI in the USA) most systems inherit the flaws of the previous solution, simply painting over the cracks, rather than take a more considered fundamental approach.

As well as looking at the fundamental fuel properties that are important to knock and detonation, this work attempts to construct a fundamentally based characterisation scheme with the potential of replacing the octane rating systems. The combined diagrams of the scheme encompass both laminar and turbulent burning, are not limited by condition or dependant on apparatus.

7.2 The reduced thermokinetic model

The model presented in chapter 2 and developed for simple fuels in chapter 3 has been shown to be capable of reproducing ignition delay times for fuels disparate to its originally intended application of PRFs.

The model is quite compact but allows sufficient parameterisation to replicate a wide variety of fuels for ignition delay time.

The capabilities of the scheme are stretched when tasked with excitation time, but of some consolation is the H_2/CO profile in chapter 3, which has simpler chemistry and lower auto-ignition delay times than either of the other fuels tested. The general trend

across fuels is a closer approximation to excitation times as the size of fuel molecule reduces, or more appropriately, as the auto-ignition delay time becomes small.

The inability of the single stage reduced scheme to produce good excitation times with a sufficiently small time step may be an indication that the chemistry in the excitation time region is markedly different to that of the auto-ignition delay period.

A preliminary attempt at a more suitable form of reduced model for excitation time has been made. This model separates the reaction into two distinct stages, separated by the point of ignition. The pre-ignition stage is adjusted for low heat release rates while maintaining an accurate τ_i, while the post-ignition stage has much higher heat release rates associated with the excitation period.

The two stage scheme was able to reproduce τ_e data produced by comprehensive modelling much more closely than the single stage scheme, coming within 1 order of magnitude as opposed to 3.

The use of the same reactions for both stages in the scheme was mandated by the remaining intermediate species at the point of ignition. This has the consequence of introducing an artificial NTC region in the resulting τ_e Arrhenius curve, a feature not present in the comprehensive scheme data.

7.3 Combustion Diagrams

The two complimentary diagrams developed through chapters 4, 5 and 6 represent a potentially comprehensive method for characterisation for fuels, and at least a comparative characterisation for engines.

The existing diagram of Bradley et al. (2002) (Fig. 4.2) has been developed and shown to be much more broadly applicable than originally thought. The original diagram was intended only to apply to a single fuel air mixture and across a very narrow condition set. The computational data of Peters et al. (2015) was able to verify that the diagram also applies to both n-heptane and i-octane at differing conditions. This was further verified by the addition of experimental data for which sufficient data was available (Bates et al., 2016).

Of note is the resistance to detonation of methane, CH_4, which does not enter the detonation peninsula until relatively high temperatures and pressures are reached. In addition, CH_4 is gaseous at atmospheric conditions, so does not experience the potential problems of liquid fuels such as formation of droplets and subsequent mixing with oil. This suggests that CH4 might have potential as a fuel for internal combustion engines, including CAI engines.

In the original diagram laminar burning is assessed through ignition at a hot spot. The diagram is indicative of ignition intensity and able to identify many combustion regimes in isolation. The *U*/*K* diagram concentrates on turbulent combustion, but auto-ignitive parameters have been used to link it to the ε/ξ diagram and increase the capabilities of both. Through this link, for example, potentially lucrative combustion regimes for CAI engines have been identified.

The least certainty in the diagrams lies with the parameter ε, which is indicative of the heat release available to reinforce the pressure pulse from reaction. This group requires some attention to improve certainty and better define the bounds of the existing diagrams.

7.4 Future Research

The most notable areas for future work are related to excitation time. Most of the uncertainty in the detonation peninsula is related to the two variables of hot spot radius and excitation time.

Further work with comprehensive modelling is required to obtain reliable excitation time data for increasingly large fuel molecules. There may be some controversy surrounding the accuracy of even comprehensive modelling in this regard, but the impossibility of measurement with current techniques make the comprehensive models an important approach.

Reduced modelling of excitation time is also an area of interest. While detailed schemes more reliable, and even a prerequisite to the reduced scheme for a given fuel, the extremely small time steps involved make detailed modelling within applications such as CFD prohibitive. The presented scheme is very much in its infancy and shows some obvious shortcomings. The transition between the pre-ignition stage of auto-ignition and the major heat release of the excitation time requires further attention to remove artefacts of the former, such as NTC, from the latter. Additionally, the use of the same basic scheme construction between the two reaction stages seems unnecessary; the excitation stage is apparently simpler, with no visible NTC. The excitation stage of reaction might be better modelled by a simpler scheme consisting of just reactions *R1* and *R2* of the original scheme, the high temperature reaction pathway. Alternately, an entirely new scheme for the excitation period might be necessary.

Also in doubt is the general construction and formation of a real hot spot. This work uses estimated dimensions based on the geometry of an assumed engine at TDC, and

sweeping simplifications are made with regard to the reactivity gradients involved. Greater understanding of how hot spots are formed, and their geometries and properties would be a great asset in better understanding phenomena such as detonation.

Application of the two-diagram approach to fuels of increasing interest such as alcohols ethanol and n-butanol is of interest, as the reduction of fossil fuel usage remains a priority. Alcohols are already being introduced as additives to gasoline in many parts of the world, and the alcohol content of fuel only looks likely to increase. It also seems unlikely that the real fuels of the future will be simple pure fuels, rather a blend of constituent fuels tailored to provide desirable combustion and storage properties. Application of the U/K and ξ/ε diagrams should not be restricted to pure fuels but also applied to blends, such as those of TRFs, a common formulation for a gasoline surrogate. Promising alternative fuels that have some undesirable property, such as n-butanol, which is prone to condensation due to a high vapour pressure, are also good candidates for blending in order to alleviate that undesirable property. In this example, the blending of n-butanol in itself reduces its concentration and makes condensation less likely. The two-diagram approach should be extended to engines, both CAI and SI. Here it might be useful in identifying contributing factors to knock, or methods to remedy them.

The applications of the two-diagram approach discussed so far have been automotive in focus. The approach might equally be applied to such fields as hazards in the storage or transportation of fuels or their uses in fields such as power generation.

The global applicability of the ξ/ε diagram is the subject of some doubt for P. Dai et al. (2016). Currently only a few fuels and conditions have been used to define the

boundaries of the detonation peninsula. Studies to define the peninsula boundaries using additional fuels over a wide range of conditions are needed to determine the reliability of a boundary that is intended to be globally applicable. The ideal candidate for this type of study would appear to be CH_4, which has reasonably well understood kinetics and is of some interest due to its apparent high resistance to detonation as shown on the present detonation peninsula, Fig. 4.6.

Better understanding the hot spot, the root cause of detonations, combined with continued development of the dimensionless diagrams shown here, and an improved understanding of excitation time and its chemistry are all important factors to be considered for future work.

8 Appendix 1

8.1 The Reduced Model applied to CFD

The following constant volume explosion equations were obtained:

$$\frac{d}{dt}Y_F = -k_1 Y_F - k_{3\mathrm{F}} Y_F \frac{Y_{O2}\rho}{W_{O2}} \frac{Y_Y \rho}{W_Y} \left(\frac{p}{p_0}\right)^{-2.2} + k_{3\mathrm{B}} \frac{Y_I}{W_I} \left(\frac{p}{p_0}\right)^{-3.5} - \frac{k_5}{2} \frac{Y_{O2}}{W_{O2}} \frac{Y_Y \rho}{W_Y}$$

$$\frac{d}{dt}Y_{O2} = -ak_2 \frac{Y_X}{W_X} X_{O2} \rho \frac{\rho}{\bar{W}} - 2\mathrm{k}_{3\mathrm{F}} \frac{Y_F}{W_F} Y_{O2} \rho \frac{\rho}{\bar{W}} \left(\frac{p}{p_0}\right)^{-2.2} + 2\mathrm{k}_{3\mathrm{B}} \frac{Y_I}{W_I} \left(\frac{p}{p_0}\right)^{-3.5}$$

$$-(a-1)k_5 Y_{O2} \frac{Y_Y \rho}{W_Y}$$

$$\frac{d}{dt}Y_Y = 2\mathrm{k}_4 \frac{Y_I}{W_I} - k_5 \frac{Y_{O2}}{W_{O2}} Y_Y \rho$$

$$\frac{d}{dt}Y_I = k_{3\mathrm{F}} \frac{Y_F}{W_F} \frac{Y_{O2}\rho}{W_{O2}} \frac{\rho}{\bar{W}} \left(\frac{p}{p_0}\right)^{-2.2} - k_{3\mathrm{B}} Y_I \left(\frac{p}{p_0}\right)^{-3.5} - k_4 Y_I$$

$$\frac{d}{dt}Y_X = k_1 \frac{Y_F}{W_F} - k_2 Y_X \frac{Y_{O2}\rho}{W_{O2}} \frac{\rho}{\bar{W}}$$

Where $\bar{W}$ is the mean molecular mass (kg/mol) of the mixture and is assumed to be constant through the course of the reaction, W_N is molecular mass of the species, and ρ is density. p/p_0 is the ratio of pressure to reference pressure and the pressure dependence of the model is determined by the index of this ratio where present. The reference pressure is taken to be 1 MPa or 1.10^6 bar.

The system of equations also contains the energy equation, which can be similarly

obtained. The resulting equation is derived as:

$$d\frac{\rho e}{dt} = -\left[k_1 \frac{Y_F \rho}{W_F}\left(\frac{p}{p_0}\right)^{0.5} h_1\right] - \left[k_2 \frac{Y_X \rho}{W_X}\frac{Y_{O2}\rho}{W_{O2}}\frac{\rho}{\bar{W}} h_2\right] - \left[k_{3\mathrm{F}} \frac{Y_F \rho}{W_F}\frac{Y_{O2}\rho}{W_{O2}}\frac{\rho}{\bar{W}}\left(\frac{p}{p_0}\right)^{-2.2} h_{3\mathrm{F}}\right] - \left[k_{3\mathrm{B}} \frac{Y_I \rho}{W_I}\left(\frac{p}{P_0}\right)^{-3.5} h_{3\mathrm{B}}\right] - \left[k_4 \frac{Y_I \rho}{W_I} h_4\right] - \left[k_5 \frac{Y_{O2}\rho}{W_{O2}}\frac{Y_Y \rho}{W_Y} h_5\right]$$

Where $h_n = H_N/\bar{W}$ is specific enthalpy with units kJ/kg and e (kJ/kg) is the specific internal energy.

8.2 Reduced model species for CFD

Species	i-Octane	W (g/mol)	n-Heptane	W (g/mol)
F	i-C_8H_{18}	114.2	C_7H_{16}	100.2
I	$OC8H_{15}O_2H + H_2O$	96.6	$OC_7H_{13}O_2H$	146.21
X	$3C_2H_4 + CH_2 + CH_3 + H$	19.04	$3C_2H_4 + CH_3 + H$	20.04
Y	OH	17.01	OH	17.01
P	$8CO_2 + 9H_2O$	38.19	$7CO_2 + 8H_2O$	38.14
O_2	O_2	32	O_2	32
N_2	N_2	14.01	N_2	14.01

Table 8.1: Species for use in CFD with reduced model

9 References

R.G. Abdel-Gayed, Derek Bradley, F.K.-K. Lung, *Combustion regimes and the straining of turbulent premixed flames*, Combustion and Flame, Volume 76, Issue 2, May 1989, Pages 213-218

Akihisa, D. and Daisaku, S., "*Research on Improving Thermal Efficiency through Variable Super-High Expansion Ratio Cycle*," SAE Technical Paper 2010-01-0174, 2010, doi:10.4271/2010-01-0174.

Allen, J. and Law, D.: "*Advanced Combustion Using a Lotus Active Valve Train: Internal Exhaust Gas Recirculation Promoted Auto-Ignition*", Proceedings of the IFP International Congress 2001, p.p. 85-100, (2001).

ASTM D2700-16a, Standard Test Method for Motor Octane Number of Spark-Ignition Engine Fuel, ASTM International, West Conshohocken, PA, 2016, www.astm.org

ASTM D2699-16, Standard Test Method for Research Octane Number of Spark-Ignition Engine Fuel, ASTM International, West Conshohocken, PA, 2016, www.astm.org

References

L. Bates, D. Bradley, G. Paczko, N. Peters, “Engine Hot Spots: Modes of Auto-ignition and Reaction Propagation," Combust. Flame 166 (2016) 80-85.

Bates, L., Bradley, D. *Deflagrative, auto-ignitive, and detonative propagation regimes in engines* (2017) Combustion and Flame, 175, pp. 118-122.

Bhari, A., *A Rapid Compression Machine with the Novel Concept of Crevice Containment,* in *Department of Engineering* 2010, University of Akron: Akron.

D. Bradley, R.A. Hicks, M. Lawes, C.G.W. Sheppard, R. Woolley, *The Measurement of Laminar Burning Velocities and Markstein Numbers for Iso-octane–Air and Iso-octane–n-Heptane–Air Mixtures at Elevated Temperatures and Pressures in an Explosion Bomb*. Combust. Flame 115 (1998) 126-144.

Bradley, D. and Morley C. 1997, “*Autoignition in Spark-Ignition Engines*” In Compton, R.G. ed, Hancock, G. ed, Pilin, M.J. ed, *Comprehensive Chemical Kinetics*. Elsevier

Bradley, D., Morley, C., Gu, X., and Emerson, D., "*Amplified Pressure Waves During Autoignition: Relevance to CAI Engines*," SAE Technical Paper 2002-01-2868, 2002, doi:10.4271/2002-01-2868.

D. Bradley, *Autoignitions and detonations in engines and ducts*. Phil. Trans. Royal Soc. A 370 (2012) 689-714.

References

Bradley, D., *Combustion and the design of future engine fuels.* Proceedings of the Institution of Mechanical Engineers, Part C: Journal of Mechanical Engineering Science, 2009. **223**(12): p. 2751-2765.

D. Bradley, R.A Head, *Engine autoignition: The relationship between octane numbers and autoignition delay times*. Combust. Flame 147 (2006) 171-184.

D. Bradley, G.T. Kalghatgi, *Influence of autoignition delay time characteristics of different fuels on pressure waves and knock in reciprocating engines*. Combust. Flame 156 (2009) 2307-2318.

D. Bradley M. Lawes, Kexin Liu, M.S. Mansour, MS *Measurements and correlations of turbulent burning velocities over wide ranges of fuels and elevated pressures*. Proc. Combust. Inst. 34 (2013) 1519–1526.

Bradley, D., Lawes, M. & Mansour, M.S. *The Problems of the Turbulent Burning Velocity*. Flow Turbulence Combust (2011) 87: 191.

Bourdon, A., Rymer, G., and Wanker, R., "*Optimization of a 5-Step Kinetic Scheme for HCCI Applications*," SAE Technical Paper 2004-01-0559, 2004, doi:10.4271/2004-01-0559.

References

Brands, T., Hottenbach, P., Koss, H., Grunefeld, G. et al., "*Effects of Mixture Stratification on Ignition and Combustion in a GCAI Engine*," SAE Int. J. Engines 7(2):714-729, 2014, doi:10.4271/2014-01-1270.

S. Browne, Z. Liang, J.E. Shepherd, *Detailed and simplified chemical reaction mechanisms for detonation simulation.* Fall 2005 Western States Section of the Combustion Institute (2005).

Liming Cai, Heinz Pitsch, Samah Y. Mohamed, Venkat Raman, John Bugler, Henry Curran, S. Mani Sarathy, *Optimized reaction mechanism rate rules for ignition of normal alkanes*, Combustion and Flame, Volume 173, November 2016, Pp 468-482, ISSN 0010-2180

Chaos, M. and F.L. Dryer, *Chemical-kinetic modeling of ignition delay: Considerations in interpreting shock tube data.* International Journal of Chemical Kinetics, 2010. 42(3): p. 143-150.

Peng Dai , Zheng Chen , Shiyi Chen , Yiguang Ju , *Numerical experiments on reaction front propagation in n -heptane/air/mixture with temperature gradient*, Proc. Combust. Inst. 35 (2014) 3045–3052 .

Chengken Qi, Peng Dai, Hao Yu, Zheng Chen, *Different modes of reaction front propagation in n-heptane/air mixture with concentration non-uniformity*, Proceedings

of the Combustion Institute, Available online 22 June 2016, ISSN 1540-7489, http://dx.doi.org/10.1016/j.proci.2016.06.086.

D.F. Davidson, M.M. Gauthier, R.K. Hanson, *Shock tube ignition measurements of iso-octane/air and toluene/air at high pressures*. Proc. Combust. Inst. 30 (2005) 1175-1182.

Dahnz, C., Han, K., Spicher, U., Magar, M. et al., *"Investigations on Pre-Ignition in Highly Supercharged SI Engines,"* SAE Int. J. Engines 3(1):214-224, 2010, doi:10.4271/2010-01-0355.

Dingle, S., Cairns, A., Zhao, H., Williams, J. et al., *"Lubricant Induced Pre-Ignition in an Optical SI Engine,"* SAE Technical Paper 2014-01-1222, 2014, doi:10.4271/2014-01-1222.

Dry, M. E. *The Fischer–Tropsch process*: 1950–2000.*Catal. Today*, 2002, **71**, 227.

K. Fieweger, R. Blumenthal , G. Adomeit ,*Self-ignition of S.I. engine model fuels: a shock tube investigation at high pressure*, Combust. Flame 109 (1997) 599–619.

Fraser, N., Blaxill, H., Lumsden, G., and Bassett, M., "Challenges for Increased Efficiency through Gasoline Engine Downsizing," *SAE Int. J. Engines* 2(1):991-1008, 2009, doi:10.4271/2009-01-1053.

References

Tien Mun Foong, Kai J. Morganti, Michael J. Brear, Gabriel da Silva, Yi Yang, Frederick L. Dryer, *The octane numbers of ethanol blended with gasoline and its surrogates*, Fuel, Volume 115, January 2014, Pages 727-739

Fujimoto, K., Yamashita, M., Hirano, S., Kato, K. et al., *"Engine Oil Development for Preventing Pre-Ignition in Turbocharged Gasoline Engine,"* SAE Int. J. Fuels Lubr. 7(3):869-874, 2014, doi:10.4271/2014-01-2785.

I. Gorbatenko, University of Leeds, Private communication (2016).

Griffiths, J.F. and J.A. Barnard, *Flame and Combustion*. 3rd ed. 1996, London: Blackie Academic & Professional.

X.J. Gu, D.R. Emerson, D. Bradley, *Modes of reaction front propagation from hot spots.* Combust. Flame 133 (2003) 63–74.

Halstead, M., Prothero, A. and Quinn, C. P., *A Mathematical Model of the Cool-Flame Oxidation of Acetaldehyde* Proc. R. Sot. Lond. A322,377 (1971).

Halstead, M. P., Prothero, A. & Quinn, C. P. *Modeling the ignition and cool-flame limits of acetaldehyde oxidation* Combust. Flame 20, 211 (1973).

References

Halstead, M. P., Kirsch, L. J., Prothero, A., andQuinn, C. P., *A Mathematical Model for Hydrocarbon Autoignition at High Pressures.* Proc. Roy. Soc. A346, 515 (1975).

Halstead, M., Kirsch, L. J. and Quinn, C. P., *The Autoignition of Hydrocarbon Fuels at High Temperatures and Pressures-Fitting of a Mathematical Model* Combust. Flame, 30,45 (1977).

Hirano, S., Yamashita, M., Fujimoto, K., and Kato, K., "Investigation of Engine Oil Effect on Abnormal Combustion in Turbocharged Direct Injection - Spark Ignition Engines (Part 2)," SAE Technical Paper 2013-01-2569, 2013, doi:10.4271/2013-01-2569

Kalghatgi, G., *"Fuel Anti-Knock Quality- Part II. Vehicle Studies - How Relevant is Motor Octane Number (MON) in Modern Engines?,"* SAE Technical Paper 2001-01-3585, 2001, doi:10.4271/2001-01-3585.

G.T. Kalghatgi, *Developments in internal combustion engines and implications for combustion science and future transport fuels*. Proc. Combust. Inst. 35 (2015) 101-115.

References

G.T. Kalghatgi, D. Bradley *Pre-ignition and 'super-knock' in turbo-charged spark-ignition engines* International Journal of Engine Research Vol 13, Issue 4, (2012) 399 – 414

G.T. Kalghatgi, D. Bradley, J. Andrae, A.J. Harrison, *Internal Combustion Engines: Performance, Fuel Economy and Emissions*. (2009) IMechE London, UK, 8-9 December 2009, Institution of Mechanical Engineers.

Kirsch, L. J. and Quinn, C. P., Sixteenth Symposium (International) on Combustion**,** p. 233, The Combustion Institute, Pittsburgh (1976).

H. Kobayashi , T. Tamura , K. Maruta , T. Niioka , F.A. Williams , *Burning velocity of turbulent premixed flames in a high pressure environment*, Symp. (Int.) Com- bust. 26 (1996) 389–396 .

Law, D., Allen, J., Kemp, D. and Williams, P.: *"4-Stroke Controlled Auto Ignition Investigations Using a Single Cylinder Engine With Lotus Active Valve Train (AVT)"*, Proceedings of the 21st century Emissions Technology Conference, IMechE Paper No. C588/006/2000, (2000).

Lee, C., Vranckx, S., Heufer, K., et al. *On the Chemical Kinetics of Ethanol Oxidation: Shock Tube, Rapid Compression Machine and Detailed Modelling Study*. Zeitschrift

für Physikalische Chemie International Journal of Research in Physical Chemistry and Chemical Physics, (2011). 226(1), pp. 1-28.

Lee, D. and S. Hochgreb, *Hydrogen Autoignition at Pressures Above the Second Explosion Limit (0.6-4.0 MPa).* International Journal of Chemical Kinetics, 1998. **30**(6): p. 385-406.

Tie Li, Yi Gao, Jiasheng Wang, Ziqian Chen, *The Miller cycle effects on improvement of fuel economy in a highly boosted, high compression ratio, direct-injection gasoline engine: EIVC vs. LIVC, Energy Conversion and Management*, Volume 79, March 2014, Pages 59-65

Livengood J.C., Wu P.C., (1955), '*Correlation of autoignition phenomena in internal combustion engines and rapid compression machines'*, Symposium (International) on Combustion, 5:347-356.

A.E. Lutz, R.J. Kee, J.A. Miller, H.A. Dwyer, A.K. Oppenheim, *Dynamic effects of autoignition centers for hydrogen and C1, 2-hydrocarbon fuels*. Twenty-Second Symposium (International) on Combustion/the Combustion Institute (1988) pp. 1683-1693.

References

A.B. Mansfield, M.S. Wooldridge, *High-pressure low-temperature ignition behavior of syngas mixtures.* Combust. Flame 161 (2014) 2242-2251.

P.W. Manz, VW Germany, Private Communication (Bradley, 2012)

J.W. Meyer, A.K. Oppenheim, *On the shock-induced ignition of explosive gases*, Symp. (Int.) Combust. 13 (1971) 1153–1164.

Miller, C., "*Roles of Detonation Waves and Autoignition in Spark - Ignition Engine Knock as Shown by Photographs Taken at 40,000 and 200,000 Frames Per Sec,"* SAE Technical Paper 470207, 1947, doi:10.4271/470207.

N. Morgan, A. Smallbone. A. Bhave, M. Kraft, R. Cracknell, G. Kalghatgi, *Mapping surrogate gasoline compositions into RON/MON space*. Combust. Flame 157 (2010) 1122-1131.

Muller, U.C. and N. Peters, *Global Kinetics for n-Heptane Ignition at High Pressures.* Symposium (International) on Combustion, 1992. **99**(3-4): p. 533-540.

Nakashima, T., Saito, K., Basaki, M., and Furuno, S., *"A Study of Stratified Charge Combustion Characteristics in New Concept Direct Injection SI Gasoline Engine,"* SAE Technical Paper 2001-01-0734, 2001, doi:10.4271/2001-01-0734

References

N. Peters, B. Kerschens, G. Paczko, *Super-Knock Prediction Using a Refined Theory of Turbulence.* SAE paper 2013-01-1109, (2013).

N. Peters, G. Paczko, H. Pitsch, *Wall film evaporation causing pre-ignition in turbocharged gasoline engines*, 25th International Colloquium on the Dynamics of Explosions and Reactive Systems Leeds, 2015 .

M.I. Radulescu , G.J. Sharpe, C.K. Law, J.H.S. Lee , *The hydrodynamic structure of unstable cellular detonations*, J. Fluid Mech. 580 (2007) 31–81 .

M.I. Radulescu, H.D. Ng, J.H.S. Lee, B. Varatharajan, *The effect of argon dilution on the stability of acetylene/oxygen detonations,* Proc. Combust. Inst 29 (2002) 2825–2831.

A. Robert, S. Richard, O. Colin, T. Poinsot, *LES study of deflagration to detonation mechanisms in a downsized spark ignition engine*. Combust. Flame 162 (2015) 2788-2807.

P. Rothenberger, GM Powertrain, Germany, Private Communication (Bradley, 2012).

References

J. Rudloff, J.M. Zaccardi, S. Richard, J.M. Anderlohr, Proc. Combust. Inst.34 (2013) 2959-2967. Proc. Combust. Inst.34 (2013) 2959-2967.

R. Sankaran, Hong. G. Im, E.R. Hawkes, J.H. Chen, *The effects of non-uniform temperature distribution on the ignition of a lean homogeneous hydrogen–air mixture.* Proc. Combust. Inst. 30 (2005) 875-882.

M. Schreiber; A. S. Sakak; A. Lingens; J. Griffiths, *A reduced thermokinetic model for the autoignition of fuels with variable octane ratings*, Symp. (Int.) Combust. 25 (1994) pp 933-940.

Sczomak, D. and Patterson, G., *"Overview of Central-Injection Air-Assisted SIDI Technology Emissions and Fuel Consumption,"* SAE Technical Paper 2003-01-0545, 2003, doi:10.4271/2003-01-0545.

M. Short, G.J. Sharpe, *Pulsating instability of detonations with a two-step chain-branching reaction model: theory and numeric*, Combust. Theory Model. 7 (2003) 401–416.

G. P. Smith, D. M. Golden, M. Frenklach, N. W. Moriarty, B. Eiteneer, M. Goldenberg, C. T. Bowman, R. K. Hanson, S. Song, W. C. Gardiner Jr, GRI-Mech 3.0, (1999). Available: http://www.me.berkeley.edu/gri_mech (accessed 15/05/2016).

Takeuchi, K., Fujimoto, K., Hirano, S., and Yamashita, M., *"Investigation of Engine*

References

Oil Effect on Abnormal Combustion in Turbocharged Direct Injection - Spark Ignition Engines," SAE Int. J. Fuels Lubr. 5(3):1017-1024, 2012, doi:10.4271/2012-01-1615.

Kimitoshi Tanoue, Yuichi Chado, Taishu Jimoto, Takashi Nomura, Fumio Shimada, Jun Hashimoto, *Effect of autoignition characteristics of fuels on knocking properties.* International J of Engine Research September 1, (2015) 1468087415601785.

Turner, JWG, Popplewell, A, Patel, R et al. (17 more authors) (2014) *Ultra Boost for Economy: Extending the Limits of Extreme Engine Downsizing.* SAE International Journal of Engines, 7 (1). 2014-01-1185. 387 - 417. ISSN 1946-3936

Turns, S.R., *An Introduction to Combustion*. 2nd ed. (2006), New York: Mc Graw Hill.

V.N. Voevodsky , R.I. Soloukhin, *On the mechanism and explosion limits of hydrogen-oxygen chain self-ignition in shock waves*, Symp. (Int.) Combust. 10 (1965) 279–283 .

Watanabe, Y., et al., *Evaluation of Homogeneous Charge Compression Ignition at High Engine Speeds Using a Super Rapid Compression Machine*, in *Powertrains, Fuels and Lubricants Meeting*2008, SAE International: Rosemont, Illinois.

White, D.R., *Influence of diaphragm opening time on shock-tube flows.* Journal of Fluid Mechanics, 1958. **4**(06): p. 585-599.

References

Wurmel, J. and J.M. Simmie, *CFD studies of a twin-piston rapid compression machine.* Combustion and Flame, 2005. **141**(4), p. 417-430.

Yeo, J., *Autoignition in Gasoline Engines*, in *Department of Mechanical Engineering*1994, University of Leeds, Leeds.

Chun Sang Yoo, Tianfeng Lu, Jacqueline H. Chen, Chung K. Law, *Direct numerical simulations of ignition of a lean n-heptane/air mixture with temperature inhomogeneities at constant volume: Parametric study*. Combust. Flame 158 (2011) 1727-1741.

Ya B. Zel'dovich, *Regime classification of an exothermic reaction with nonuniform initial conditions.* Combust. Flame 39 (1980) 211-214.

Zahdeh, A., Rothenberger, P., Nguyen, W., Anbarasu, M. et al., "Fundamental Approach to Investigate Pre-Ignition in Boosted SI Engines," *SAE Int. J. Engines* 4(1):246-273, 2011, doi:10.4271/2011-01-0340.